


## Article

# Exploring Growth of *Mycobacterium smegmatis* Treated with Anticarcinogenic Vanadium Compounds

Zeyad Arhouma <sup>1,2</sup>, Heide A. Murakami <sup>2</sup>, Jordan T. Koehn <sup>2</sup>, Xiaorong Li <sup>2,3</sup>, Deborah A. Roess <sup>1,4</sup>, Dean C. Crick <sup>1,5</sup> and Debbie C. Crans <sup>1,2,\*</sup> 

<sup>1</sup> Cellular and Molecular Biology, Colorado State University, Fort Collins, CO 80523, USA; zkrahuma@rams.colostate.edu (Z.A.); deborah.roess@colostate.edu (D.A.R.); dean.crick@colostate.edu (D.C.C.)

<sup>2</sup> Department of Chemistry, Colorado State University, Fort Collins, CO 80523, USA; heide.murakami@colostate.edu (H.A.M.); jordan\_koehn@med.unc.edu (J.T.K.); henryqian2013@gmail.com (X.L.)

<sup>3</sup> College of Pharmaceutical Sciences, Southwest University, Chongqing 400715, China

<sup>4</sup> Departments of Biomedical Sciences, Colorado State University, Fort Collins, CO 80523, USA

<sup>5</sup> Mycobacteria Research Laboratories, Department of Microbiology, Immunology and Pathology, Colorado State University, Fort Collins, CO 80523, USA

\* Correspondence: debbie.crans@colostate.edu

**Abstract:** A major problem with patient treatments using anticancer compounds is accompanying bacterial infections, which makes more information on how such compounds impact bacterial growth desirable. In the following study, we investigated the growth effects of an anticarcinogenic non-toxic Schiff base oxidovanadium(V) complex (*N*-(salicylideneaminato)-*N'*-(2-hydroxyethyl)ethane-1,2-diamine) coordinated to the 3,5-di-*tert*-butylcatecholato ligand on a representative bacterium, *Mycobacterium smegmatis* (*M. smeg*). We prepared the Schiff base V-complexes as reported previously and selected a few complexes to develop a V-complex series. Biological studies of *M. smeg* growth inhibition were complemented by spectroscopic studies using UV-Vis spectrophotometry and NMR spectroscopy to determine which complexes were intact under biologically relevant conditions. We specifically chose to examine (1) the growth effects of Schiff base oxidovanadium complexes coordinated to a catechol, (2) the growth effects of respective free catecholates on *M. smeg*, and (3) to identify complexes where the metal coordination complex was more potent than the ligand alone under biological conditions. Results from these studies showed that the observed effects of Schiff base V-catecholate complex are a combination of catechol properties including toxicity, hydrophobicity, and sterics.

**Keywords:** Schiff base vanadium-catechol complexes; Mycobacteria; speciation; NMR spectroscopy; UV-Vis spectroscopy; growth inhibition; tuberculosis



**Citation:** Arhouma, Z.; Murakami, H.A.; Koehn, J.T.; Li, X.; Roess, D.A.; Crick, D.C.; Crans, D.C. Exploring Growth of *Mycobacterium smegmatis* Treated with Anticarcinogenic Vanadium Compounds. *Inorganics* **2022**, *10*, 50. <https://doi.org/10.3390/inorganics10040050>

Academic Editors: Bernhard Spingler and Isabel Correia

Received: 28 December 2021

Accepted: 29 March 2022

Published: 2 April 2022

**Publisher's Note:** MDPI stays neutral with regard to jurisdictional claims in published maps and institutional affiliations.



**Copyright:** © 2022 by the authors. Licensee MDPI, Basel, Switzerland. This article is an open access article distributed under the terms and conditions of the Creative Commons Attribution (CC BY) license (<https://creativecommons.org/licenses/by/4.0/>).

## 1. Introduction

The power of metal complexes as anticancer agents, with the best examples being Pt-based compounds such as cisplatin, carboplatin, and oxaliplatin, has been demonstrated in clinical settings over several decades [1–9]. In addition to Pt-based compounds, a number of other metal-based compounds have been reported to have anticancer properties including Ru-containing anticancer compounds [10], Cu-containing anticancer compounds [11], vanadium-containing compounds [12,13], and other transition metal-based compounds [14–20]. Although the compounds that make it to the clinic are highly effective, patients treated with anticancer agents are very susceptible to bacterial infections [11,21–24]. Microbial infections can be very serious; some have been reported to modulate host cell transformation and hence promote the production of carcinogenic metabolites participating in inflammation responses, to disrupt cell metabolism, and to modify genomic or epigenetic

characteristics [21–24]. Reducing the potential problems prompting patient evaluation and intravenous administration of broad spectrum antibiotics is critically important and may represent a practice difference for the patient [21–24]. Thus, information on the effects of anticarcinogenic compounds on various bacterial strains are of general interest.

When evaluating effects of metal complexes on bacterial cells, it is, however, important to consider that these compounds are coordination complexes and many of these compounds do not remain intact during study due to their inherent hydrolytic instability in complex biological media [25–29]. In addition, the effects of the metal complex versus its ligand can be important, particularly in cases where the ligand has potent effects on the cells being studied [28,30–32]. Here, we use a recently identified anti-cancer compound, a Schiff base vanadium-based catecholato complex (oxidovanadium(IV) complexed to *N*-(salicylideneaminato)-*N'*-(2-hydroxyethyl)ethane-1,2-diamine 3,5-di-*tert*-butylcatecholato ligand) [33,34], which was found to be significantly more potent than cisplatin in several cancer lines including glioma multiforme, an aggressive brain cancer (T98g), lung cancer cells (A549), and pancreas cancer cells (PANC-1) [34]. Because this vanadium compound is uniquely more stable than generally observed for Schiff base V(V) catecholato complexes, this class of compounds has been proposed for targeted injections directly into tumors [34]. In this study, we also investigate a number of related vanadium complexes (V-complexes) containing known, non-innocent catecholato ligands to determine whether there are identifiable relationships between effects of the metal complex on bacterial growth and complex stability in bacterial growth media. For those complexes that do not remain intact, biological effects of the resulting products including the non-innocent ligand is of considerable interest.

Table 1 shows a summary of studies in which the V-complex, the ligand, and free metal ion were evaluated in different bacteria, fungi, or pathogens [32,35–39]. Although vanadate was reported to inhibit growth of *Mycobacteria smegmatis* (*M. smeg*) some time ago [40], we have recently demonstrated that cell growth of *M. smeg* is much more sensitive to the large compact decavanadate anion ( $V_{10}$ -anion) than the smaller vanadate monomer ( $HVO_4^{2-}$ ,  $V_1$  anion) [41]. Furthermore, replacing one of the V-atoms in the  $V_{10}$  cluster to form a monosubstituted polyoxidovanadate affects growth inhibition with the order being  $V_{10} > V_9Pt > V_9Mo$  [42]. The sensitivity of *M. smeg* to monosubstituted polyanions further motivated studies here examining cell growth effects for a number of related intact and hydrolyzed coordination complexes with non-innocent ligands in this representational bacterial system.

The structure of the classes of coordination complexes where both complexes and ligands have previously been investigated in bacteria are listed in Figure 1 [28,32,35–38]. The compounds reported include complexes with hydrazones [35], Schiff bases [36], quinolones [32], and related studies with phenanthrolines [28] and Vitamin E-hydroxylamino-Triazine ligands [30]. Several phenanthroline complexes have been studied extensively in cancer cells (Table 1); because the ligand has been shown to have variable effects depending on time of treatment, it serves as an excellent comparison for these studies carried out in bacteria [28]. Previous studies demonstrate that compounds are sensitive to the oxidation state of the metal ion and the ligand as well as the nature of the coordination complexes. It is, however, important to note that both the biological and chemical systems investigated made direct comparisons difficult [43]. Generally, complexes formed by hydrazones and Schiff bases were found to be more potent than their ligands [35,36], while compounds formed from quinolones were less potent than their respective ligands [32]. Recently, we identified a non-toxic Schiff base oxidovanadium(V) complex (*N*-(salicylideneaminato)-*N'*-(2-hydroxyethyl)ethane-1,2-diamine) containing a hydrophobic and sterically hindered catecholato ligand (3,5-di-*tert*-butylcatecholato ligand) which is effective against several cancer cell types including glioma multiforme, an aggressive brain cancer (T98g), lung cancer cells (A549), pancreas cancer cells (PANC-1), cultured human bone cancer cells, breast cancer (MDA-MB-231), and human foreskin fibroblasts (HFF-1) [33,34,44,45]. Several catecholato ligands have been reported to be toxic [46–48] and, as a result, either more

or less potent than their parent vanadium complexes [32,33]. In contrast to the parent catecholate, the sterically hindered catechol 3,5-di-tert-butylcatechol in a complex has been reported to be less toxic in female Swiss mice [45]. To obtain more information on the effects of intact complexes versus ligands, we selected a group of complexes with varying stability that contained a ligand such as a catechol with the potential to inhibit *M. smeg* growth.

**Table 1.** Previous studies of the effect of various V-complexes in other microorganisms.

Vanadium Complexes	Microorganism (a, b, c)	Inhibitory Activity	Results	References
$M_2[CH_2(V^VO_2(sal-bhz))_2] \cdot 2H_2O$ $M_2[CH_2(V^VO_2(sal-fah))_2] \cdot 2H_2O$ <b>M = K<sup>+</sup> or Cs<sup>+</sup> for sal-bhz</b> (5,5'-methylbis(salicylaldehyde) and benzoylhydrazide); <b>M = K<sup>+</sup> for sal-fah</b> (5,5'-methylbis(salicylaldehyde) and 2-furoylhydrazide)	<b>Protozoa:</b> <i>Entamoeba histolytica</i>	IC <sub>50</sub> values between 0.36 and 2.32 µM	Complexes had potent antibacterial activity compared to hydrazone ligand	[35]
$[VO(L)_2(H_2O)]SO_4$ <b>L = 1-phenyl-2,3-dimethyl-4-(1H-indole-3-carboxaldehyde)-3-pyrazolin-5-one (HL).</b>	<b>Bacteria:</b> <i>Staphylococcus aureus</i> <sup>a</sup> , <i>Klebsiella pneumoniae</i> <sup>b</sup> , <i>Legionella monocytogenes</i> <sup>b</sup> , <i>Escherichia coli</i> , <i>Pseudomonas aeruginosa</i> <sup>b</sup> , and <i>Salmonella typhimurium</i> <sup>b</sup> <b>Fungi:</b> <i>Candida albicans</i> and <i>Aspergillus flavus</i>	IC <sub>50</sub> values between 16 and 64 µg/mL	Complexes had potent antibacterial activity compared to Schiff base ligand	[36]
<b>Complexes with 8-hydroxyquinoline (8HQ)</b>	<b>Bacteria:</b> <i>Mycobacterium tuberculosis</i>	IC <sub>50</sub> values between 2.9 and 42.23 µM	Complexes had less potent activity compared to 8-hydroxyquinoline (8HQ) ligand	[32]
<b>V(IV)O(Salophen)</b> $[VO(C_{20}H_{16}N_4O_2)] \cdot H_2O$	<b>Parasite:</b> <i>Leishmania amazonensis</i>	IC <sub>50</sub> values of 3.51 µM and 6.65 µM	Complexes had more potent activity compared to H <sub>2</sub> Salophen ligand	[37]
<b>Complexes with chlorido-substituted hydrazone ligands ([VOL(OEt)(EtOH)]</b>	<b>Bacteria:</b> <i>Bacillus subtilis</i> <sup>a</sup> , <i>Staphylococcus aureus</i> , <i>Escherichia coli</i> , and <i>Pseudomonas fluorescens</i> <sup>b</sup> <b>Fungi:</b> <i>Candida albicans</i> and <i>Aspergillus niger</i>	MICs values at 1.2 and >150 µg/mL	Complexes have stronger activities compared to the free chloride hydrazones	[38]
<b>(3Hpca)<sub>4</sub>[H<sub>2</sub>V<sub>10</sub>O<sub>28</sub>] · 2H<sub>2</sub>O · 2(3-pca); (complex I)</b> <b>(4-Hpca)<sub>4</sub>[H<sub>2</sub>V<sub>10</sub>O<sub>28</sub>] · 2(4-pca); (complex II)</b>	<b>Bacteria:</b> <i>Escherichia coli</i>	GI <sub>50</sub> values at 0.47 and 0.67 mmol L <sup>-1</sup>	Cation increases toxicity	[39]
<b>Complexes formed with 1,10-phenanthroline or 4,7-dimethyl-1,10-phenanthroline ligands</b>	<b>Cancer cells<sup>c</sup>:</b> Ovarian, cisplatin sensitive A2780, breast MCF7, and prostate PC3		Complexes have variable potency comparable with effects of free phenanthroline ligands and duration of treatment	[28]

Table 1. Cont.

Vanadium Complexes	Microorganism (a, b, c)	Inhibitory Activity	Results	References
Complexes with Vitamin E-hydroxylamino-Triazine Ligands	Cancer cells: Human Cal33 cells, Hela cells, embryonic mouse fibroblasts (NIH/3T3)		Complexes are less toxic than free ligands for all three cell lines	[30]

<sup>a</sup> Gram-positive bacteria; <sup>b</sup> Gram-negative bacteria; <sup>c</sup> cancer cell lines (A2780, MCF7, and PC3).

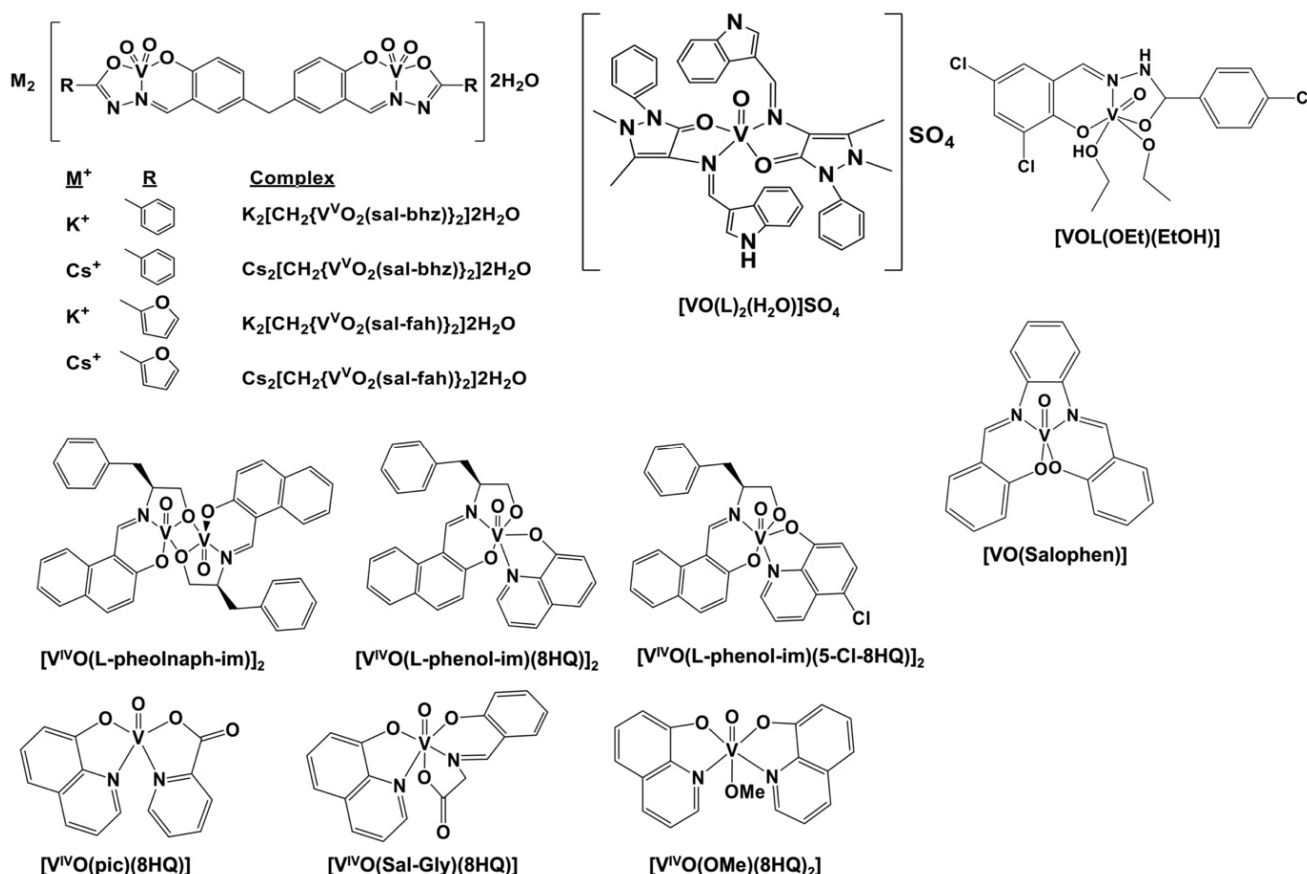


**Figure 1.** The structure of the classes of coordination complexes where activity of both the complex and ligand was investigated in bacteria [32,35–38].

## 2. Results

### 2.1. Compound Design

We first investigated the effects of a series of Schiff base vanadium(V) catecholato compounds related to the oxidovanadium(V) complex (*N*-(salicylideneaminato)-*N'*-(2-hydroxyethyl)ethane-1,2-diamine) which exhibits potent anticancer properties [33,34,44] and is shown in Figure 2. The varying effects of these compounds on *M. smeg* growth of each vanadium complexes were compared to the effects of its free ligands (see results below as they are described and in Figures S1–S3). The complexes selected for investigation contained non-innocent ligands or formed complexes with different electronic properties. We selected the known V-scaffold  $[VO_2(Hshed)]$ , the most potent anti-cancer agent  $[VO(Hshed)(dtb)]$ , and control compounds with different electronic properties of the parent  $[VO(Hshed)(cat)]$ , and two compounds with electronic withdrawing ligands  $[VO(Hshed)(tbc)]$  and  $[VO(Hshed)(4NO_2)]$ . In addition, we designed here three new complexes, the hydrophobic  $[VO(Hshed)(Coum)]$ , and a complex with an electron withdrawing ligand –CN,  $[VO(Hshed)(CN)]$ , and a complex with an electron donating ligand OMe,  $[VO(Hshed)(OMe)]$ .

[VO(Hshed)(3OMet)] (see Figures S4–S19). In selecting this series of compounds, we expected varying degrees of complex stability in H<sub>2</sub>O and in 7H9 media. The stability and speciation of the complexes was investigated using NMR and UV-Vis spectroscopy and the data are provided in the Supplementary Materials (Figures S20–S31).

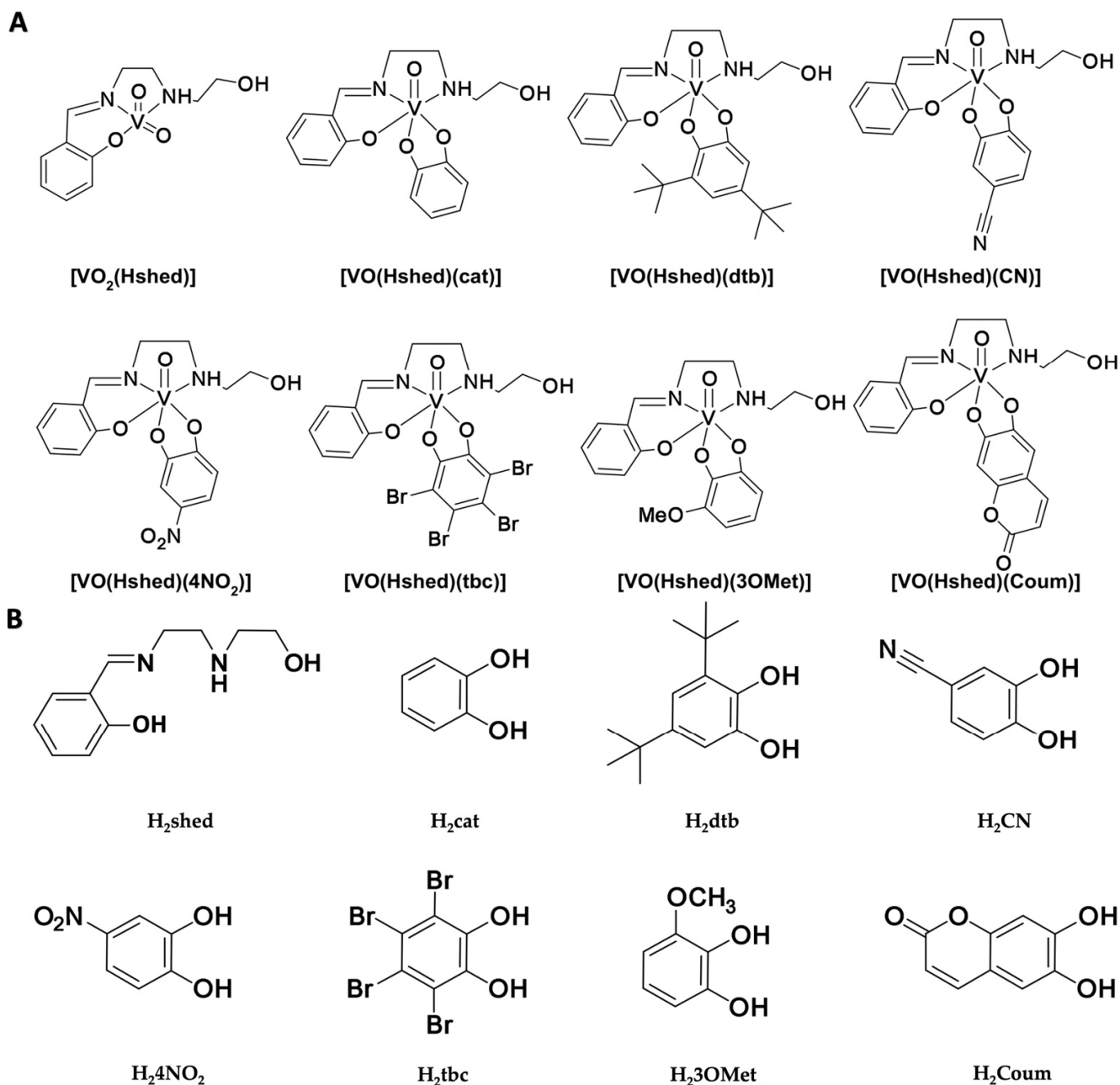


**Figure 2.** The schematic formulas for the (A) vanadium complexes and (B) free catechol ligands.

## 2.2. Growth Inhibition of Vanadium Complexes and Free Ligands Determined Using the Minimum Inhibitory Concentration (MIC)

The biological activity of V-complexes and free ligands was investigated in terms of their respective antibacterial effects on the growth of *M. smeg* by measuring IC<sub>50</sub> values. The growth inhibition data of *M. smeg* treated with three different V-complexes and free catechol ligands are shown in Figure 3 including (a) [VO(Hshed)(dtb)] and H<sub>2</sub>dtb, (b) [VO(Hshed)(tbc)] and H<sub>2</sub>tbc, and (c) [VO(Hshed)(cat)] and H<sub>2</sub>cat. The IC<sub>50</sub> values and the growth inhibition curves for the effects of the additional V-complexes, their free catechol,



and the Schiff base V-Hshed scaffold on the bacterial growth are shown in Figures S1 and S2. It was necessary to use DMSO to dissolve hydrophobic compounds into solution for preparation of stock solutions. For studies with *M. smeg*, the stock solution was diluted with cell medium to prepare a solution containing 10% DMSO which was then diluted via serial dilution to lower V-complex concentrations containing less DMSO. To clarify the role of DMSO in cell studies, cell growth inhibition up to 20% DMSO was evaluated and was significant. The effects of DMSO alone on the growth of *M. smeg* is shown in Figure S3. When cells were treated with 10% DMSO alone, the highest DMSO concentration used in our studies of V-compound effects on *M. smeg* growth, growth inhibition was reduced to values that were still significant but markedly lower than seen for 20% DMSO. For compounds that were present in serially diluted medium and contained less than 10% DMSO, there were insignificant effects of DMSO on *M. smeg* growth indicating that the IC<sub>50</sub> values for all the complexes and catechols tested were due to compound effects and not to the presence of DMSO (Table 2).

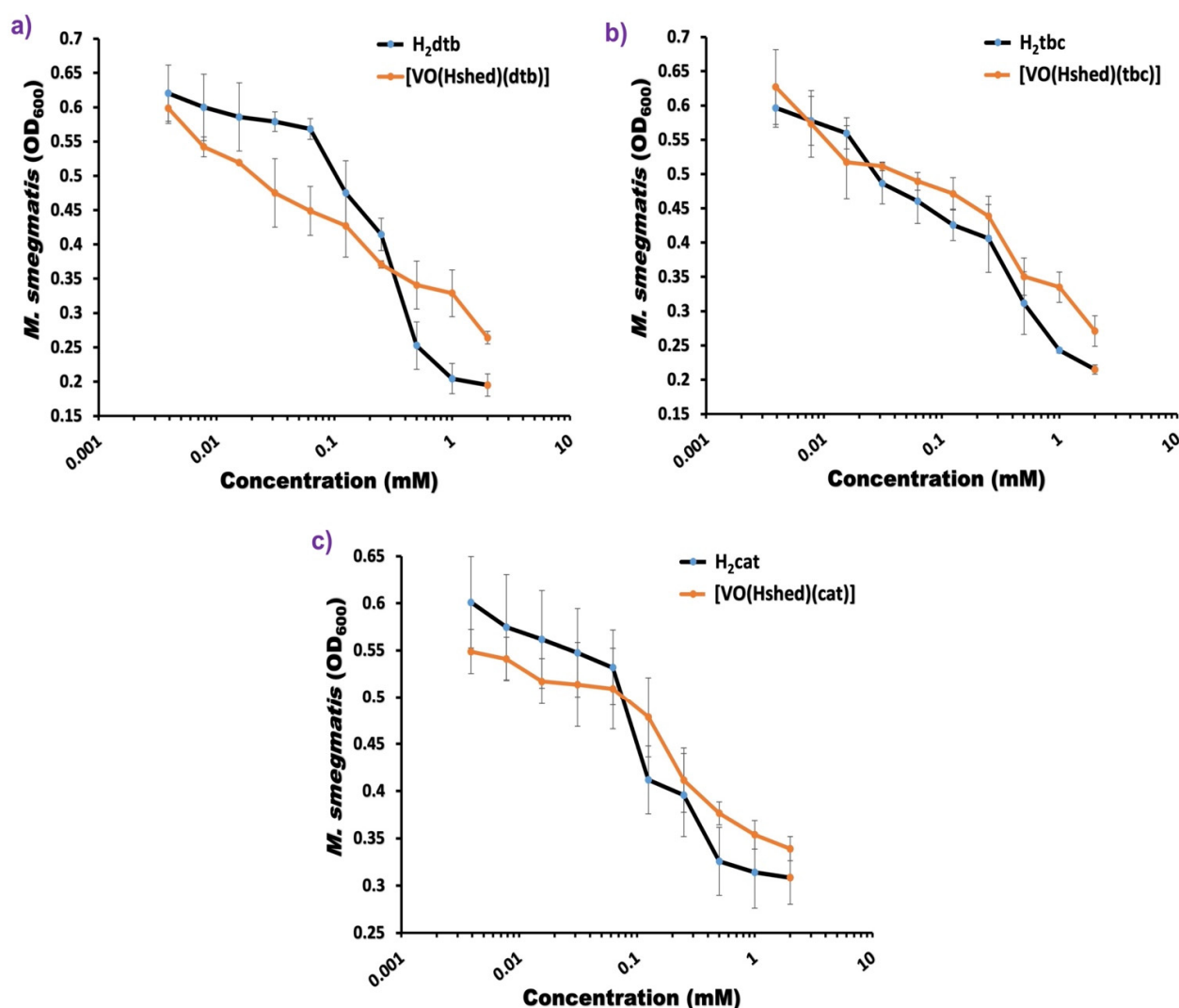


**Figure 3.** Histograms showing the growth of *M. smeg* treated with (a) [VO(Hshed)(dtb)] and H<sub>2</sub>dtb, (b) [VO(Hshed)(tbc)] and H<sub>2</sub>tbc, and (c) [VO(Hshed)(cat)] and H<sub>2</sub>cat using concentrations ranging from 0.004 to 2.00 mM. Error bars are the standard deviation for triplicate measurements.

**Table 2.** Antibacterial activity ( $IC_{50}$ ) of Schiff base vanadium complexes, the Schiff base [VO<sub>2</sub>Hshed] scaffold, and free catechols against *M. smeg* at 0.250 mM.

Tested Compounds	$IC_{50}$ ( $\mu$ M)	The Effect of Complexes Compared to the Free Catechol
[VO(Hshed)(dtb)] H <sub>2</sub> dtb	119 $\pm$ 0.09 241 $\pm$ 0.07	2 $\times$ more potent in terms of concentration
[VO(Hshed)(Coum)] H <sub>2</sub> Coum	370 $\pm$ 0.13 506 $\pm$ 0.28	1.4 $\times$ more potent in terms of concentration
[VO(Hshed)(4NO <sub>2</sub> )] H <sub>2</sub> 4NO <sub>2</sub>	472 $\pm$ 0.02 610 $\pm$ 0.05	1.3 $\times$ more potent in terms of concentration
[VO(Hshed)(tbc)] H <sub>2</sub> tbc	449 $\pm$ 0.22 416 $\pm$ 0.19	Same effect in terms of concentration
[VO(Hshed)(cat)] H <sub>2</sub> cat	518 $\pm$ 0.29 109 $\pm$ 0.05	5 $\times$ less potent in terms of concentration
[VO(Hshed)(3OMet)] H <sub>2</sub> 3OMet	555 $\pm$ 0.23 262 $\pm$ 0.15	2 $\times$ less potent in terms of concentration
[VO(Hshed)(CN)] H <sub>2</sub> CN	608 $\pm$ 0.07 447 $\pm$ 0.04	1.4 $\times$ less potent in terms of concentration
[V(O) <sub>2</sub> (Hshed)]	516 $\pm$ 0.31	Schiff base V-complex scaffold

The  $IC_{50}$  values of V-complexes and their free ligands are shown in Table 2. Although all of the V-complexes and their free ligands were comparatively weak growth inhibitors of *M. smeg*, differences in growth inhibition were observed between the V-complex and its free ligand. The  $IC_{50}$  of [VO(Hshed)(dtb)], [VO(Hshed)(Coum)], and [VO(Hshed)(4NO<sub>2</sub>)] indicated that these compounds were more potent in inhibiting bacterial growth with an  $IC_{50}$  of 119, 370, and 472  $\mu$ M, respectively. In complexes, their ligands showed 2-, 1.4-, and 1.3-fold more growth inhibition than did the free ligands. [VO(Hshed)(cat)], [VO(Hshed)(3OMet)], and [VO(Hshed)(CN)] showed less inhibitory activity against the bacterial growth with an  $IC_{50}$  of 518, 555, and 608  $\mu$ M, respectively, when compared with their free ligands. Finally, the  $IC_{50}$  of [VO(Hshed)(tbc)] had a similar activity, an  $IC_{50}$  of 449  $\mu$ M, when compared with its free ligand with an  $IC_{50}$  of 416  $\mu$ M.

### 2.3. Solution Chemistry and Stability of Vanadium-Catechol Complexes in Reference Solutions and in Growth Media as Monitored by UV-Vis Spectroscopy

To further investigate whether the observed effects of compounds or their ligands on *M. smeg* growth in cell culture were related to complex stability, spectroscopic studies were undertaken. We examined the V-compounds in three different solutions. (1) Simple H<sub>2</sub>O-DMSO containing no other additives, (2) 7H9-DMSO media with nutrients for *M. smeg* growth but without other additives, and (3) 7H9 media in which *M. smeg* had grown and the media contained bovine serum albumin (BSA), oleic acid, and dextrose and from which cells had then been removed (referred to as “supernatant”). UV-Vis studies and subsequent NMR spectroscopic studies would show which compounds remained intact and for how long. The stability of the V-compounds was not expected to be the same in these three solutions nor was the response of each compound to these conditions likely to be the same.

First, the V-catechol complexes with different ligands were analyzed using UV-Vis spectroscopy to explore the speciation and the stability of these complexes in both in H<sub>2</sub>O:DMSO and in 7H9:DMSO at 37 °C. Here, 7H9 medium was used in *M. smeg* growth studies which made its effects on compound speciation and stability of particular interest. The samples were initially dissolved in DMSO due to the low solubility of the compounds and their weak growth inhibition. Hence, the stabilities of the compounds described differ here from studies of compound stability reported in cancer cell lines studies where the compound concentration and temperature were lower and there was less DMSO present in the original stock solution [33]. To conserve space, the spectra of the complexes

shown in Figure 4 were recorded in 7H9:DMSO at 37 °C, while the UV-Vis spectra of complexes in H<sub>2</sub>O:DMSO and in supernatant:DMSO are presented in Supplementary Materials (Figures S20 and S21). Because of the dilution of the original compound stock solution to 0.250 mM V-compound with H<sub>2</sub>O or 7H9 media, the DMSO content decreased from 50% in the stock solution to about 6% for the UV-Vis studies.

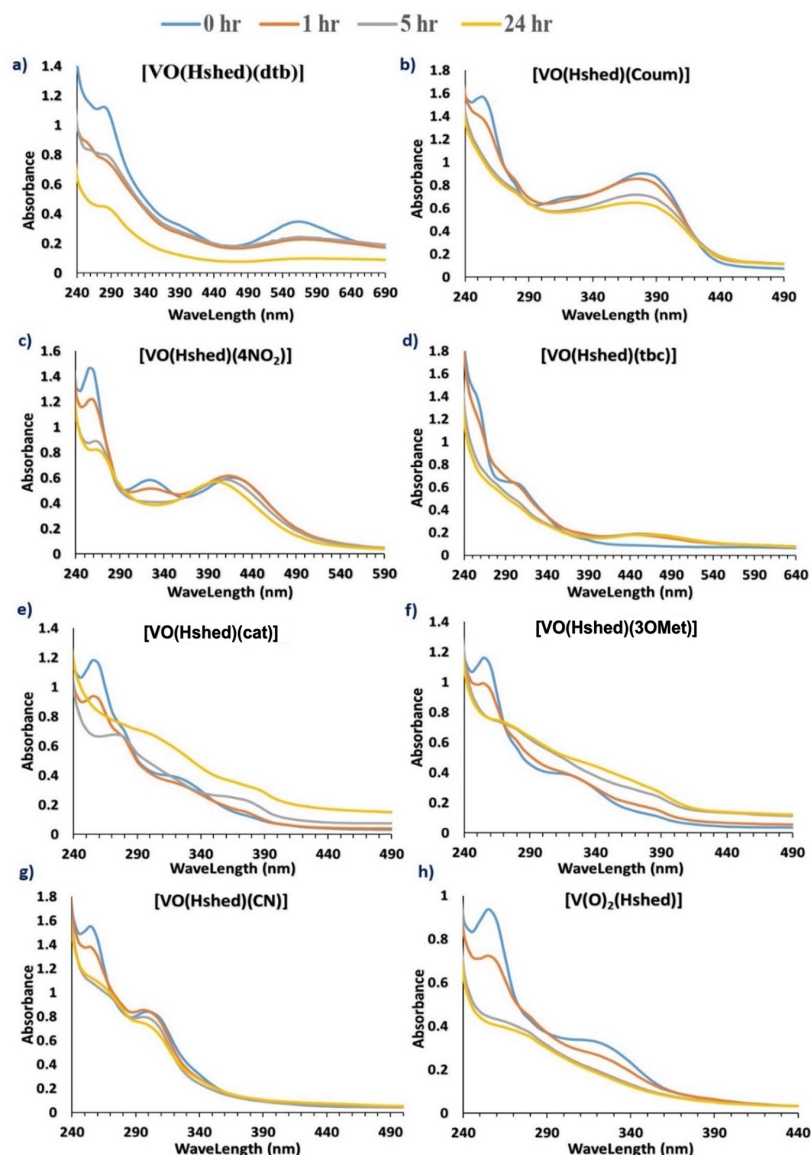


**Figure 4.** UV-Vis spectra for all of the complexes at 0.250 mM in 7H9:DMSO as a function of time (0, 1, 5, 24 h). The compounds from which the spectra (a–h) are listed above each of the spectra.

UV-Vis spectroscopy can be used to show time-dependent changes in complex structure and hence complex stability. The spectra of complexes and of free ligands at time zero ( $t = 0$ ) in H<sub>2</sub>O:DMSO and in 7H9:DMSO were recorded as reference for the spectra in 7H9:DMSO and are shown in Supplementary Materials (Figure S22) as well as summarized in Table 3. For comparison, the stability of the Schiff base oxido-vanadium(V) complex scaffold, [VO<sub>2</sub>(Hshed)], which provided the basic framework for all the complexes in this series, was also evaluated. The main absorption peaks were observed at wavelengths at 255 and 325 nm in aqueous solution and were similarly observed in 7H9 media. The addition of catechol ligands, as expected, added additional signals to the complexes with shifts that depended on the electronic properties of the catechol.



**Table 3.** UV-Vis parameters observed from the Schiff base V-catecholate complexes and free catecholate ligands at  $t = 0$  h with 0.250 mM V-compound at 37 °C <sup>a</sup> in the mixed solutions (94:6 H<sub>2</sub>O:DMSO or 94:6 7H9 medium:DMSO).

Complex	Complex (H <sub>2</sub> O/DMSO) Absorbance (nm)/ $\epsilon$ ( $\times 10^3$ M <sup>-1</sup> )	Complex (7H9/DMSO) Absorbance (nm)/ $\epsilon$ ( $\times 10^3$ M <sup>-1</sup> )
[VO(Hshed)(dtb)]	(280, 1.161, 4.6); (565, 0.396, 1.6)	(280, 1.123, 4.5); (565, 0.347, 1.4)
[VO(Hshed)(Coum)]	(255, 1.344, 5.3); (275, 0.727, 2.9); (370, 0.870, 3.5)	(255, 1.562, 6.2); (280, 0.836, 3.3); (325, 0.678, 2.7); (380, 0.901, 3.6)
[VO(Hshed)(4NO <sub>2</sub> )]	(255, 1.299, 5.2); (325, 0.533, 2.1); (405, 0.552, 2.2)	(260, 1.445, 5.8); (325, 0.583, 2.3); (420, 0.568, 2.3)
[VO(Hshed)(tbc)]	(255, 0.854, 3.4); (310, 0.284, 1.1)	(305, 0.613, 2.5)
[VO(Hshed)(cat)]	(255, 0.951, 3.8); (280, 0.579, 2.3); (375, 0.117, 0.47)	(255, 1.183, 4.7); (280, 0.743, 3.0); (325, 0.349, 1.4); (380, 0.138, 0.55)
[VO(Hshed)(3OMet)]	(255, 0.831, 3.3); (280, 0.408, 1.6)	(255, 1.162, 4.6); (325, 0.441, 1.8); (385, 0.156, 0.62)
[(VO(Hshed)(CN)]	(255, 1.473, 5.9); (300, 0.666, 2.7)	(255, 1.55, 6.2); (300, 0.789, 3.2)
[V(O) <sub>2</sub> (Hshed)]	(255, 0.682, 2.7); (325, 0.200, 0.80)	(255, 0.937, 3.7); (325, 0.312, 1.2)
[H <sub>2</sub> dtb] ligand	(280, 0.218, 0.90)	(280, 0.513, 2.1)
[H <sub>2</sub> Coum] ligand	(255, 0.371, 1.5); (300, 0.524, 2.1); (345, 0.972, 3.9)	(295, 0.639, 2.6); (350, 0.939, 3.8)
[H <sub>2</sub> 4NO <sub>2</sub> ] ligand	(310, 0.652, 2.6); (350, 0.784, 3.1)	(265, 0.726, 2.9); (320, 0.575, 2.3); (430, 0.767, 3.1)
[H <sub>2</sub> tbc] ligand	(275, 0.241, 1.0); (300, 0.203, 0.81)	(255, 0.941, 3.8); (300, 0.574, 2.3)
[H <sub>2</sub> cat] ligand	(275, 0.364, 1.5)	(275, 0.642, 2.6)
[H <sub>2</sub> 3OMet] ligand	(270, 0.137, 0.50)	(270, 0.417, 1.7)
[H <sub>2</sub> CN] ligand	(250, 1.172, 4.7); (290, 0.453, 1.8)	(250, 1.293, 5.2); (290, 0.792, 3.2)

<sup>a</sup> Prepared from 10 mM V-complex stock solutions (50:50 H<sub>2</sub>O:DMSO) and 50:50 7H9:DMSO.

The UV-Vis spectra of [VO(Hshed)(dtb)] exhibited two absorption bands at 280 nm (sh) and 565 nm (m) in water and two major signals at 280 and 565 nm in 7H9:DMSO. Both the signal for the free H<sub>2</sub>dtb catechol ligand at 280 nm (Figure S5) and the signal at 565 nm decreased at the 1 h time point and were gone at the 5 h timepoint. This indicated that the compound was present initially in 7H9 media but, as shown in Figure 4, began to hydrolyze. However, there are some differences in the spectra. For [VO(Hshed)(4NO<sub>2</sub>)], [VO(Hshed)(tbc)], and [VO(Hshed)(CN)], there is a signal around 300–330 nm suggesting some isomer formation for these V-compounds. The data at the zero-time point have been summarized for all the complexes (nm, absorbance, and extinction coefficient) and are listed in Table 3.

The UV-Vis spectra of [VO(Hshed)Coum] had main absorption peaks at wavelengths of 255 nm (m), 280 nm (sh), and 385 nm (m) in aqueous solution and, in 7H9 media, an extra peak of 325 nm (sh). This additional peak in 7H9 media indicated the formation of an additional species. The decrease of the two major species as a function of time suggested that this complex is present in solution for some time before hydrolyzing. [VO(Hshed)(4NO<sub>2</sub>)] exhibited three major signals at 255, 325, and 405 nm. During the first hour the signal at 255 and 325 nm decreased, whereas the signal at 405 nm remained at the same intensity with a small change in the location of its maximum.

The spectra for the other complexes examined indicated that the complexes remained intact briefly in 7H9 media (Figure 4) or H<sub>2</sub>O:DMSO (Supplementary Materials). However, between 1 and 5 h some remained intact for the first hour of the experiment when present at 6% DMSO concentrations and higher temperature, which showed enhanced stabilities compared to previous studies [32–34]. In addition, when compounds were examined in 7H9 media, a 280 nm peak appeared that was due to formation of free catechol.

Previously, *M. smeg* was found to excrete a material that was able to catalyze the hydrolysis of V<sub>10</sub> [41]. For this reason, we also examined the effects of the V-compounds in the supernatant of the 7H9 media in which *M. smeg* had grown. Analogous experiments were conducted in this study to determine if there was a difference from the results for media alone listed in Table 4. In this series, 0.250 mM V compounds were added to the supernatant obtained from 7H9 media after *M. smeg* growth. Data showing the stability of compounds after incubation in supernatant are shown in Supplementary Materials (Figures S24–S31). These data show that there was no significant change in speciation in supernatant obtained after *M. smeg* culture when compared to data obtained using fresh media as shown in Figure 4. However, the signal at 280 nm now indicates the presence of protein, primarily in the form of bovine serum albumin [49], although some formation of free catechol cannot be ruled out since this also yields an absorbance at 280 nm.

**Table 4.** Species observed for 10 mM Schiff base vanadium-catecholate complexes in the mixture solution (50:50 H<sub>2</sub>O:DMSO) and 50:50 7H9 growth medium:DMSO at t = 0 h.

Complex	Complex $\delta$ (DMSO) or $\delta$ (H <sub>2</sub> O/DMSO) ppm/mM/%	Complex $\delta$ (7H9 Media) ppm/mM/%	[VO <sub>2</sub> -(Hshed)] at $\delta$ /mM/%	V <sub>1</sub> at $\delta$ ppm/mM/%	V <sub>4</sub> at $\delta$ ppm/mM/%
[VO(Hshed)(dtb)]/(H <sub>2</sub> O/DMSO)	387, 353 (m)/0.43, 7.36/4.3, 73.6	–	–	–541/2.11/21.1	–557/0.10/1.0
[VO(Hshed)(dtb)]/(7H9 media)	–	394, 359 (m)/0.42, 5.45/4.2, 54.5	–	–544/4.14/41.4	–
[VO(Hshed)(Coum)]/(H <sub>2</sub> O/DMSO)	–103/1.2/12	–	–524/1.5/15	–544/7.4/74	–
[VO(Hshed)(Coum)]/(7H9 media)	–	–	–	–544/10/100	–
[VO(Hshed)(cat)]/(H <sub>2</sub> O/DMSO)	206, 196 (m)/0.73, 2.47/7.3, 24.7	–	–524/1.79/17.9	–543/5.02/ 50.2	–
[VO(Hshed)(cat)]/(7H9 media)	–	205, 193 (m)/0.32, 1.83/3.2, 18.3	–526/2.10/21.0	–544/5.74 /57.4	–
[VO(Hshed)(3OMet)]/(H <sub>2</sub> O/DMSO)	265, 254(m)/1.47, 4.63/14.7, 46.3	–	–520/0.23/2.3	–540/3.56/35.6	–560/0.11/1.1
[VO(Hshed)(3OMet)]/(7H9 media)	–	265, 253(m)/0.78, 3.15/7.8, 31.5	–	–541/6.06/60.6	–
[V(O) <sub>2</sub> (Hshed)]/(H <sub>2</sub> O/DMSO)	–	–	–524/0.0	–543/8.78/87.8	–558/1.22/12.2
[V(O) <sub>2</sub> (Hshed)]/(7H9 media)	–	–	–526/0.0	–541/9.94 /99.4	–565/0.11/1.1
[VO(Hshed)(tbc)]/(H <sub>2</sub> O/DMSO)	–470, –480/2.0, 0.5/20, 5	–	–	–544/7.4/74	–
[VO(Hshed)(tbc)]/(7H9 media)	–	–	–524/0.05/0.5	–544/9.8/98	–570/0.15/1.5
[VO(Hshed)(CN)]/(H <sub>2</sub> O/DMSO)	–460/0.1/1	–	–524/3.3/33	–544/6.6/66	–
[VO(Hshed)(CN)]/(7H9 media)	–	–480/0.05/0.5	–	–544/9.95/99.5	–
[VO(Hshed)(4NO <sub>2</sub> )]/(H <sub>2</sub> O/DMSO)	–460/0.1/1	–	–524/2.5/25	–544/6.6/66	–
[VO(Hshed)(4NO <sub>2</sub> )]/(7H9 media)	–	–	–	–544/10/100	–

#### 2.4. Solution Chemistry and Stability of Vanadium-Catechol Complexes in Reference Solution and in Cell Growth Media

The stability of vanadium complexes was also investigated at different times using <sup>51</sup>V NMR spectroscopy in DMSO:H<sub>2</sub>O, DMSO:7H9 medium, and supernatants obtained following *M. smeg* culture. The representative <sup>51</sup>V NMR spectra of 10 mM [VO(Hshed)(dtb)], [VO(Hshed)(cat)], and [V(O)<sub>2</sub>(Hshed)] in the mixture solution of H<sub>2</sub>O, DMSO (50:50, H<sub>2</sub>O:DMSO), and in 7H9 (50:50, H<sub>2</sub>O:media) are shown in Figures 5–7, respectively. The NMR spectra of 10 mM [VO(Hshed)(dtb)], [VO(Hshed)(cat)], and [V(O)<sub>2</sub>(Hshed)] in the

mixture with supernatants are shown in the Supplementary Materials (Figures S24–S26). The remaining data for the additional complexes are listed in Table 4.

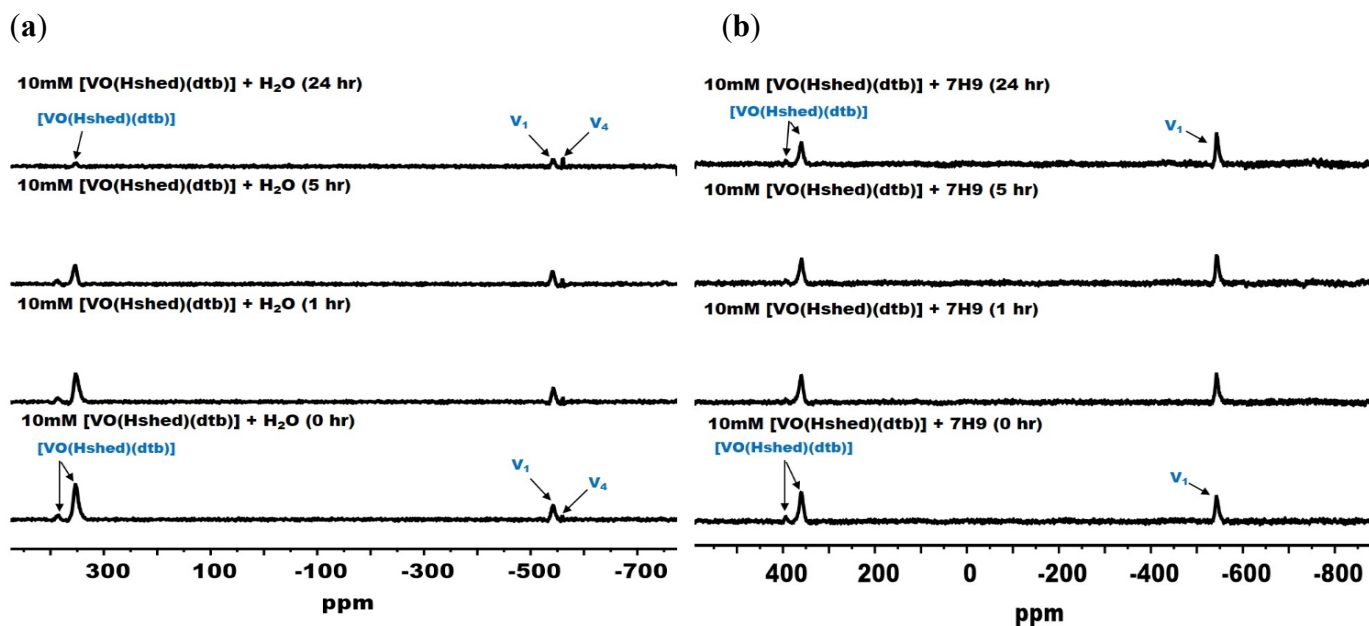


Figure 5. The  $^{51}\text{V}$  NMR spectra of 10 mM  $[\text{VO}(\text{Hshed})(\text{dtb})]$  at 0, 1, 5, and 24 h time points in (a) 50:50  $\text{H}_2\text{O}$ :DMSO and in (b) 50:50 7H9 growth medium: DMSO.

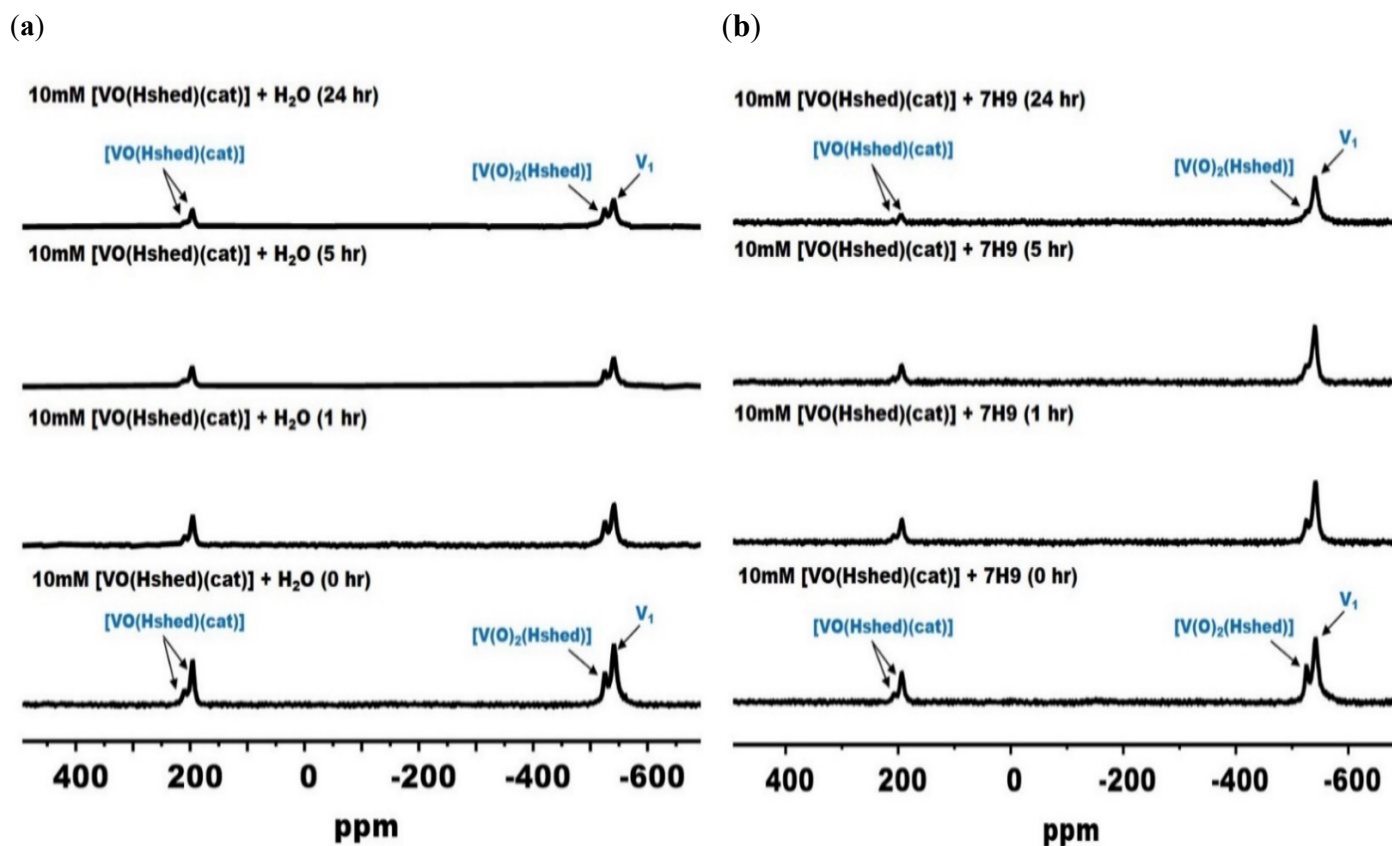
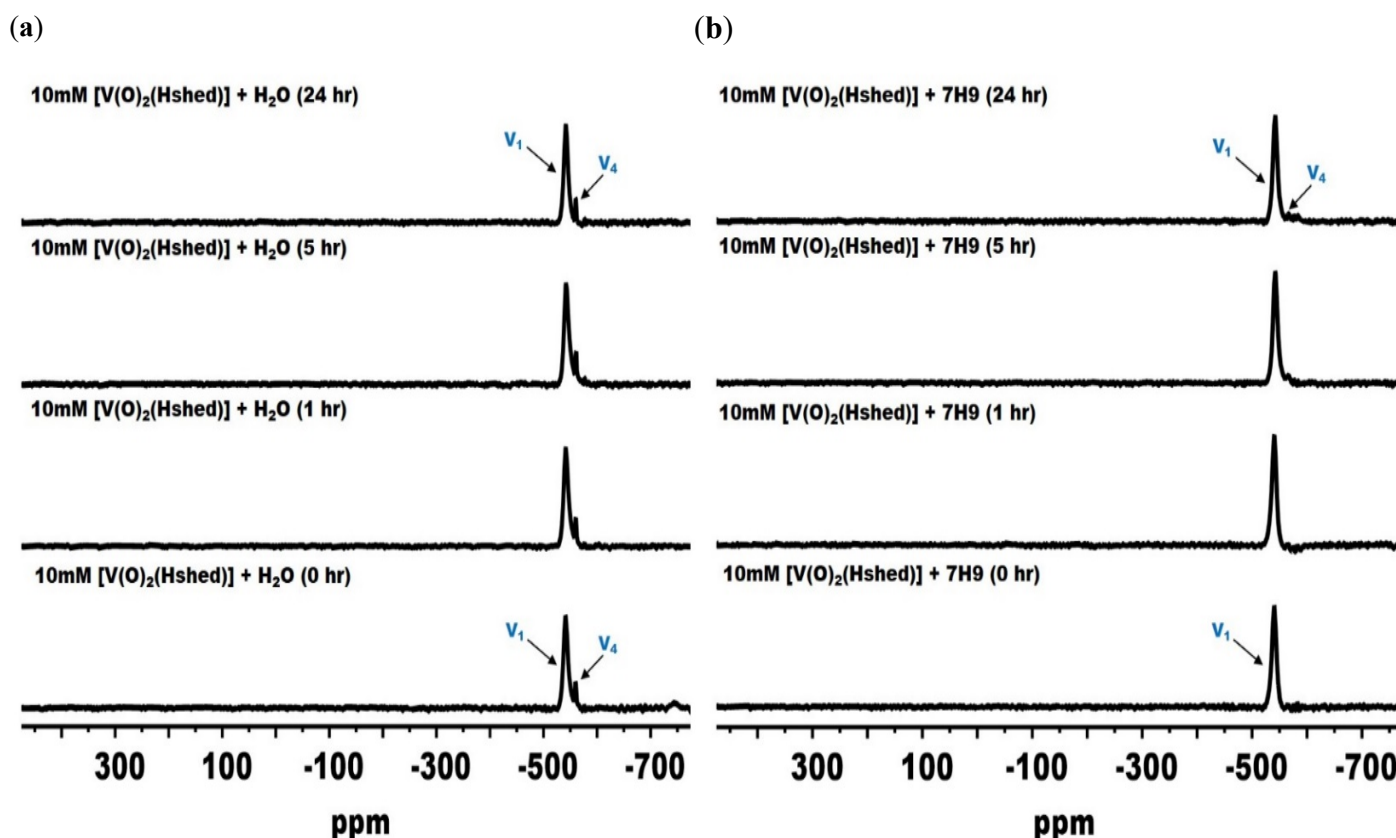


Figure 6.  $^{51}\text{V}$  NMR spectra of 10 mM  $[\text{VO}(\text{Hshed})(\text{cat})]$  at 0, 1, 5, and 24 h time points in (a) 50:50  $\text{H}_2\text{O}$ :DMSO or in (b) 50:50 7H9 growth medium:DMSO.



**Figure 7.** The  $^{51}\text{V}$  NMR spectra of 10 mM  $[\text{V}(\text{O})_2(\text{Hshed})]$  at 0, 1, 5, and 24 h time points in (a)  $\text{H}_2\text{O}$ :DMSO (50:50) and in (b) 7H9 growth medium:DMSO (50:50).

The  $^{51}\text{V}$  NMR spectra were obtained using 10 mM of  $[\text{VO}(\text{Hshed})(\text{dtb})]$  in 50:50  $\text{H}_2\text{O}$ :DMSO. Subsequently, spectra were recorded to determine how much complex remained intact at different time points when the complex was in 50:50  $\text{H}_2\text{O}$ :DMSO or in 50:50 7H9:DMSO media (Figure 5).

The spectra of  $[\text{VO}(\text{Hshed})(\text{dtb})]$  at time=0 ( $t = 0$ ) showed two peak signals assigned to  $[\text{VO}(\text{Hshed})(\text{dtb})]$  at  $\delta = 387$  and  $353$  ppm, in addition to the presence of the other two signals assigned to  $\text{V}_1$  at  $\delta = -541$  ppm and vanadate tetramer ( $\text{V}_4\text{O}_{12}^{4-}$ )  $\text{V}_4$  at  $\delta = -557$  ppm. The percentage of each species measured at the initial time point is summarized in Table 4.

Over a 24 h time period, the decrease in the  $[\text{VO}(\text{Hshed})(\text{dtb})]$  complex in  $\text{H}_2\text{O}$  was monitored by  $^{51}\text{V}$  NMR spectroscopy and an increase in  $\text{V}_1$  and  $\text{V}_4$  was observed (Figure 5a). The  $^{51}\text{V}$  NMR spectra of  $[\text{VO}(\text{Hshed})(\text{dtb})]$  in 7H9 was also recorded as a function of time. The spectrum recorded at the initial time ( $t = 0$  h) showed two complex signals at  $\delta$  (ppm) = 394 and 359 (m), in addition to one signal attributed to  $\text{V}_1$  at  $\delta = -544$  ppm. Since only small changes were observed in the spectra from 0 h, the complex is stable in the 7H9 medium (Figure 5b). The observation of the  $[\text{VO}(\text{Hshed})(\text{dtb})]$  complex in the growth assay is consistent with at least some of the observed growth effects that can be attributed to the intact  $[\text{VO}(\text{Hshed})(\text{dtb})]$  complex.

Monitoring the  $[\text{VO}(\text{Hshed})(\text{cat})]$  complex over a 24 h time period showed a decrease of the complex as a function of time in  $\text{H}_2\text{O}$  (Figure 6a). The spectrum recorded at  $t = 0$  h showed two complex signals at  $\delta$  (ppm) = 196 and 206 (m) in addition to two signals attributed to  $[\text{VO}_2(\text{Hshed})]$  at  $\delta = -524$  ppm and  $\text{V}_1$  at  $\delta = -544$  ppm. Similarly, the  $^{51}\text{V}$  NMR spectra of  $[\text{VO}(\text{Hshed})(\text{cat})]$  in 7H9 were carried out as a function of time and the two signals for the complex were also found to slowly hydrolyze in 7H9 medium (Figure 6b) to form  $[\text{VO}_2(\text{Hshed})]$  and  $\text{V}_1$ . These spectra showed that  $[\text{VO}(\text{Hshed})(\text{cat})]$  complex existed in the 7H9 growth medium, suggesting that some of the observed growth inhibition can be attributed to the intact  $[\text{VO}(\text{Hshed})(\text{cat})]$  complex.

Studies were carried out with the other complexes and these results are summarized in Table 4. For the [VO(Hshed)(Coum)] complex, a significant amount of intact complex and [VO<sub>2</sub>(Hshed)] was observed in H<sub>2</sub>O:DMSO solution in addition to V<sub>1</sub> hydrolysis product. However, all complex was hydrolyzed in 7H9 media before the <sup>51</sup>V NMR spectrum was recorded. For the [VO(Hshed)(4NO<sub>2</sub>)] complex, a trace level of complex and an intermediate species are observed in addition to a 1:5 ratio of [VO<sub>2</sub>(Hshed)] scaffold and V<sub>1</sub> hydrolysis product in H<sub>2</sub>O:DMSO. However, all complexes were hydrolyzed in 7H9 medium:DMSO before the <sup>51</sup>V NMR spectrum was recorded. For the [VO(Hshed)(CN)], a 1:3 ratio of [VO<sub>2</sub>(Hshed)] scaffold and V<sub>1</sub> hydrolysis product were observed in H<sub>2</sub>O:DMSO. However, all complexes were hydrolyzed in 7H9 medium:DMSO solution before the <sup>51</sup>V NMR spectrum was recorded. For the [VO(Hshed)(tbc)] complex, the spectra were very noisy and only trace levels of signals were observed in addition to the major peak for V<sub>1</sub>. Since this compound was investigated at the same concentrations as the other complexes, the noisy spectrum is presumably reflecting that this compound not only hydrolyzed but underwent redox chemistry at the 37 °C temperature in both H<sub>2</sub>O:DMSO and the 7H9 medium:DMSO solutions. Combined, these results show that some of these compounds are more stable than reported previously at lower temperatures and DMSO concentrations, but that several of the compounds remain unstable in 7H9 growth medium:DMSO and only hydrolyzed compounds are observed by the time the <sup>51</sup>V NMR spectra were recorded.

In Figure 7, NMR spectra are shown for the [VO(Hshed)] scaffold over a 24 h time period. These results indicate that the scaffold complex was unstable and immediately hydrolyzed to form V<sub>1</sub> within 1 h in both H<sub>2</sub>O:DMSO and 7H9:DMSO.

Select studies were carried out with the [VO(Hshed)(3OMet)] complex and the [VO(Hshed)(CN)] complex. Both hydrolyzed rapidly with little intact complex left in the solution by the time the spectra were run. This information is summarized in Table 4. These data show higher stability than reported previously in pure aqueous solution or in media used to grow cancer cells [32–34].

### 3. Discussion

The results shown in Table 2 demonstrate that complexes with reported anticancer activity have limited growth effects on *M. smeg*. However, as shown in Table 2, some complexes are more biologically active than their catechol ligand, while, for other complexes, the free catecholates are more potent growth inhibitors of *M. smeg*. Therefore, we were successful in demonstrating that within a class of compounds, biological activity can be based on subtle variations in the ligand coordinated to the vanadium.

As described in Section 1, most of the reported investigations have focused on compounds where the observed V-complex is more potent than the free ligand [35–38] or metal ion [39]. However, the quinolones and phenanthroline complexes deviate from these general observations because the free ligand is the most effective bioactive component of the complex [28,32,50]. It should be noted, however, that most of these V-quinolone complexes are difficult to evaluate because the complexes are hydrophobic and, because of their hydrophobicity, their biological activities were not evaluated under the same conditions used in aqueous assays. A careful analysis has been reported for the effects of a range of different vanadium-complexes with phenanthroline ligands in different cancer cell lines [28] and summarized in Table 1. These studies show that bioprocessing occurs after administration of these complexes and that their hydrolysis products are important for complex activity. Importantly, time-dependent responses were also observed [28] over 72 h and low concentrations of the ligand were found to be more effective than the complex [51]. Speciation is particularly important when the ligand is, by itself, a potent agent. It is also important that interactions with cellular components [27], including proteins, be considered [52,53]. Such interactions can affect delivery and uptake of both the ligand and the complex and, because of time-dependent effects, potentially produce more potent species with longer incubations [28]. These studies also underscore the importance of complex bioprocessing and the need for studies exploring effects of speciation as well as investigation of effects of



both ligands and complexes by metabolites as well as a range of proteins. Hence, we were interested in evaluating a system in which speciation and the biological effects could be determined for both the complex and free ligand.

In this study, we characterized the effects of the Schiff base V-complex scaffold as well as the catecholate ligand examined in *M. smeg* growth assays. Limited effects of the Schiff base V-complex scaffold were observed, while the catecholate ligand showed more varied growth inhibitory activity as has been reported previously [33,34]. Due to the limited water solubility of these complexes, the speciation studies were undertaken in the presence of higher concentrations of DMSO which was required to solubilize the compound for addition to the cell culture at the high concentrations needed in this study. Because the DMSO concentration was higher than those reported previously in speciation studies [33,34], the complexes were more stable than reported previously except for the [VO(Hshed)(tbc)] complex that seems to be redox active when dissolved. Temperature may also contribute to compound stability; accompanying speciation studies conducted here used the same temperature from cell studies, whereas previous studies were conducted at ambient temperature. These subtle differences in conditions may explain changes in the observed stabilities of the compounds [33,34] and are a reminder of the importance of investigating the activity of the ligands used in the complexes under consideration of conditions similar to corresponding biological studies.

The growth effects of the complexes were according to the following order: [VO(Hshed)(dtb)] > [VO(Hshed)(Coum)] > [VO(Hshed)(tbc)] > [VO(Hshed)(4NO<sub>2</sub>)] > [VO(Hshed)(cat)] = [V(O)<sub>2</sub>(Hshed)] > [VO(Hshed)(3OMet)] > [VO(Hshed)(CN)]. We anticipate that the ligand potency as a growth inhibitor is important to the overall properties of the complex as a growth inhibitor and thus determined the order of the ligand potencies. The order is H<sub>2</sub>cat > H<sub>2</sub>dtb > H<sub>2</sub>3OMet > H<sub>2</sub>tbc > H<sub>2</sub>CN > H<sub>2</sub>Coum > H<sub>2</sub>4NO<sub>2</sub>. Surprisingly, we found that H<sub>2</sub>cat was the most growth inhibiting catechol followed by H<sub>2</sub>dtb and H<sub>2</sub>3OMet. When examining the effects of the Schiff base V-complexes, only the [VO(Hshed)(dtb)] complex was found to be a potent growth inhibitor, while [VO(Hshed)(cat)] and [VO(Hshed)(3OMet)] were among the least potent complexes. This result suggests that the potency of the ligand is not one of the factors that is critical for effects by V-complexes. Hence, not only was the effect of the free catechol overcome by complex formation, but different properties were found to be important to the biological effects of these Schiff base V-complexes. It is possible that the electronic properties of the catechols are important. However, the anticipated electronic effects of substituents were H<sub>2</sub>3OMet > H<sub>2</sub>dtb > H<sub>2</sub>cat > H<sub>2</sub>tbc > H<sub>2</sub>CN > H<sub>2</sub>4NO<sub>2</sub>, while the effects of the H<sub>2</sub>Coum ligand were less predictable. Electronic effects alone cannot explain the observed effects, although they may be contributing, at least in part, to the overall activity of the complex. We have investigated the electronic effects of the complexes elsewhere but in general found that the complexes that readily undergo redox chemistry are not very stable [54]. These studies confirm the expectation that the electronic effects on the catechol ligand were not the sole factor explaining the effects of the Schiff base V-complexes or showing a pattern explaining the properties of these complexes.

As we recently reported, complex hydrophobicity [33] and the stability of the Schiff base V-complex may be important to complex activity [33,34]. Hence, it is critical to know whether the complex remains intact when assessing its observed activities in growth effects. In the present work, we chose a system in which the activities of the complexes, although weak, were compared and differences could be identified. The two most stable and hydrophobic complexes were the [VO(Hshed)(dtb)] and [VO(Hshed)(Coum)] complexes and these complexes were also found to be the most effective inhibitors of *M. smeg* growth. This result suggests that stability and hydrophobicity of the complexes should be important factors when predicting compound effects on cell growth.

Perhaps the most surprising result in this series of work here is the fact that the H<sub>2</sub>cat ligand is the catechol exhibiting the highest growth inhibitory activity. Both the H<sub>2</sub>dtb ligand and the H<sub>2</sub>Coum ligand are hydrophobic and hence are readily taken up by cells.

The H<sub>2</sub>dtb ligand is the most sterically hindered catechol. Sterics are likely to be important for complex formation because the H<sub>2</sub>dtb ligand protects the V-atom from hydrolysis, as suggested by the complexes' greater stability. From these results, we conclude that both hydrophobicity and steric hindrance are important factors for observed growth inhibition effects on *M. smeg* but that the catecholato ligand toxicity is not necessarily related to this growth effect, particularly if the complex is, at least in part, stable as was observed under the conditions of these studies.

## 4. Experimental Procedure

### 4.1. Materials

#### 4.1.1. Cell Culture Materials

The Middlebrook 7H9 Broth medium (Ref. no. 271310; Difco™) was obtained from BD Biosciences (San Jose, CA, USA) and autoclaved before use. The medium was supplemented with oleic acid (0.6% v/v; Sigma-Aldrich (St. Louis, MO, USA), 5 mg mL<sup>−1</sup> albumin (VWR), 2 mg mL<sup>−1</sup> dextrose (Sigma-Aldrich), and 10% Tyloxapol (Chem-Impex Int'l Inc (Wood Dale, IL, USA)). *Mycobacterium smegmatis* mc<sup>2</sup> 155 (*M. smeg*) has been maintained in our laboratory for some time as has been reported previously [55].

#### 4.1.2. Chemicals for Synthesis and Spectroscopic Studies

Catechol ligands were purchased from Sigma-Aldrich. Dimethyl sulfoxide (DMSO, 99.9%) was purchased from Sigma-Aldrich and deuterium oxide (D<sub>2</sub>O, 99.9%) was purchased from Cambridge Isotope Laboratories (Tewksbury, MA, USA). Reagents were used as received without further purification.

Eight Schiff base vanadium-catecholato coordination complexes were selected and prepared using procedures described initially by the Pecoraro group and described previously by our group [56–58]. DMSO was used for solubilizing the compounds for NMR spectroscopic studies and cell culture studies. Infrared spectra were obtained using a Bruker Tensor II FT-IR spectrometer (Billerica, MA, USA) in attenuated total reflectance mode with a 4 cm<sup>−1</sup> resolution.

### 4.2. Methods

#### 4.2.1. Cell Culture and Growth Conditions

*M. smeg* was cultured in Middlebrook 7H9 medium (Ref. no. 271310; Difco) supplemented with 10% OAD (oleic acid, albumin, dextrose), 0.2% (v/v) glycerol, and 10% Tyloxapol, and incubated with shaking for 24 h at 37 °C. *M. smeg* was grown to a mid-logarithmic growth phase assessed via spectrophotometry and occurred at an optical density of 0.6 at 600 nm (OD<sub>600</sub>). In some experiments where *M. smeg* was treated with vanadium complexes, the cell culture supernatant was collected for <sup>51</sup>V NMR studies.

#### 4.2.2. Minimum Inhibitory Concentration (MIC) Measurements

The inhibitory activity of the tested compounds was determined by measuring the lowest concentration that caused bacterial growth inhibition of 50% (IC<sub>50</sub>). *M. smeg* was grown to the mid-log phase of 0.6–0.8 at OD<sub>600</sub>. The final concentrations of the compounds used in these studies were obtained using serial dilutions to a final concentration range of 2 to 0.0039 mM and placed with *M. smeg* in 7H9 media into a 96-well plate. Plates were incubated for 24 h at 37 °C. A Bio-Rad Benchmark Reader (Bio-Rad Laboratories: Hercules, CA, USA) was used to check the cell viability at OD<sub>600</sub> at appropriate times. IC<sub>50</sub> was determined to be the lowest concentration of complexes that inhibited *M. smeg* growth by 50%.

#### 4.2.3. Statistical Analysis

For each treatment, data were represented as the mean and standard deviation of the IC<sub>50</sub> from triplicate measurements. The IC<sub>50</sub> was calculated using GraFit 5 data analysis software (version 5.0.13).

### 4.3. Chemistry

#### 4.3.1. Synthesis of Schiff Base Vanadium-Catecholato Coordination Complexes

The complexes were prepared from  $[\text{VO}(\text{O})_2(\text{Hshed})]$  through a condensation reaction as described by the Pecoraro group [56] and our group [57,58]. See Figure 2 for the structures of the compounds and their abbreviations. After preparation of the  $[\text{VO}_2(\text{Hshed})]$  precursor [56–58], the catechol was added to generate the complexes used in this study.  $[\text{VO}(\text{Hshed})(\text{cat})]$  [56–58];  $[\text{VO}(\text{Hshed})(\text{dtb})]$  [56–58];  $[\text{VO}(\text{Hshed})(4\text{NO}_2)]$  [56–58];  $[\text{VO}(\text{Hshed})(\text{tbc})]$  [56–58]; and three new complexes  $[\text{VO}(\text{Hshed})(\text{CN})]$ ;  $[\text{VO}(\text{Hshed})(3\text{OMet})]$ ; and  $[\text{VO}(\text{Hshed})(\text{Coum})]$ .

#### 4.3.2. Synthesis of $[\text{VO}(\text{Hshed})(\text{CN})]$

To a 250 mL round bottom Schlenk flask, acetone (100 mL) was added, which was then degassed with argon.  $[\text{VO}_2(\text{Hshed})]$  (0.290 g, 1.00 mmol) was added to the degassed acetone followed by 3,4-dihydroxybenzonitrile (0.135 g, 1.00 mmol). A deep purple solution resulted after approximately 20 s. The solution was stirred overnight under argon. The reaction mixture was vacuum filtered and then concentrated to dryness under reduced pressure at room temperature. The purple residue was dissolved in a minimal amount of acetone and then *n*-hexane (100 mL) was added. The solution was allowed to stand in a  $-20\text{ }^\circ\text{C}$  freezer overnight. The dark microcrystalline precipitate was vacuum filtered, washed with cold *n*-hexane ( $<0\text{ }^\circ\text{C}$ ,  $2 \times 25\text{ mL}$ ), and dried under vacuum for 3 days to yield 0.341 g (0.838 mmol, 84%) purple solid.  $^{51}\text{V}$  NMR (in  $\text{CD}_3\text{CN}$ ):  $-138\text{ ppm}$ ,  $-113\text{ ppm}$  (minor isomer).  $^1\text{H}$  NMR (400 MHz,  $\text{CD}_3\text{CN}$ ):  $\delta$  8.74 (s, 1H), 7.64–7.62 (dd, 1H), 7.59–7.54 (dt, 1H), 7.17–7.13 (m, 1H), 7.00–6.96 (dt, 1H), 6.91–6.88 (m, 1H), 6.83–6.80 (d, 1H), 4.23–4.18 (dd, 1H), 4.10–4.03 (dt, 1H), 3.79–3.72 (m, 1H), 3.69–3.63 (m, 1H), 3.59–3.49 (m, 2H), 3.39–3.31 (m, 1H), 3.04–2.90 (m, 2H), 2.81–2.78 (t, 1H). IR (ATR,  $4\text{ cm}^{-1}$ ): 3049 (O–H), 2218 ( $\text{C}\equiv\text{N}$ ), 1712 (Aromatic), 953 ( $\text{V}=\text{O}$ ). Calc for  $\text{C}_{18}\text{H}_{18}\text{N}_3\text{O}_5\text{V}$ : C, 53.08; H, 4.45; N, 10.32. Found: C, 52.52; H, 4.33; N, 9.96. UV-Vis peaks (in DMSO): 280 and 305 nm.

#### 4.3.3. Synthesis of $[\text{VO}(\text{Hshed})(3\text{OMet})]$

To a 250 mL round bottom Schlenk flask, acetone (100 mL) was added, which was then degassed with argon.  $[\text{VO}_2(\text{Hshed})]$  (0.290 g, 1.00 mmol) was added to the degassed acetone followed by 3-methoxy catechol (0.140 g, 1.00 mmol). A deep purple solution resulted after approximately 20 s. The solution was stirred overnight under argon. The reaction mixture was vacuum filtered and then concentrated to dryness under reduced pressure at room temperature. The purple residue was dissolved in a minimal amount of acetone and then *n*-hexane (100 mL) was added. The solution was allowed to stand in a  $-20\text{ }^\circ\text{C}$  freezer overnight. The dark microcrystalline precipitate was vacuum filtered, washed with cold *n*-hexane ( $<0\text{ }^\circ\text{C}$ ,  $2 \times 25\text{ mL}$ ), and dried under vacuum for 3 days to yield 0.280 g (0.680 mmol, 68%) purple solid.  $^{51}\text{V}$  NMR in  $\text{CD}_3\text{CN}$ : 288 ppm.  $^1\text{H}$  NMR (400 MHz,  $\text{CD}_3\text{CN}$ ):  $\delta$  8.63 (s, 1H), 7.51–7.48 (t, 1H), 6.87–6.83 (t, 1H), 6.76–6.66 (m, 2H), 6.34–6.32 (d, 1H), 6.07–6.05 (d, 1H), 5.99–5.97 (d, 1H), 3.90–3.87 (m, 3H), 3.84–3.76 (m, 2H), 3.66–3.61 (m, 2H), 3.49–3.39 (m, 1H), 3.38–3.31 (m, 1H), 2.99–2.91 (m, 1H), 2.84–2.81 (t, 1H). IR (ATR,  $4\text{ cm}^{-1}$ ): 1636 (Aromatic), 1304, 1267, 1108 (C–O), 954 ( $\text{V}=\text{O}$ ). Calc for  $\text{C}_{18}\text{H}_{21}\text{N}_2\text{O}_6\text{V}$ : C, 52.43; H, 5.13; N, 6.79. Found: C, 52.26; H, 5.17; N 6.30. UV-Vis peaks (in DMSO): 280, 335, 390, and 565 nm.

#### 4.3.4. Synthesis of $[\text{VO}(\text{Hshed})(\text{Coum})]$

The following reaction was carried out under argon atmosphere, typically using a Schlenk line to set up the reaction, followed by an argon balloon during the reaction. The  $\text{H}_2\text{Coum}$  (0.196 g, 1.10 mmol, recrystallized from benzene) and solid  $\text{VO}_2(\text{Hshed})$  (0.290 g, 1.0 mmol) were added to a 100 mL round bottom Schlenk flask followed by absolute ethanol (50 mL). The conversion of the yellow  $\text{VO}_2(\text{Hshed})$  to the purple/black  $\text{VO}(\text{Hshed})(\text{Coum})$  occurred over 4 h (colors changed from light yellow to brown to dark purple). However, the mixture was allowed to stir covered overnight under argon after which time the dark

purple reaction mixture was cooled in a dry ice/acetone bath for 1 min and then was vacuum filtered, leaving a purple black solid on the filter paper. The solid was washed twice with cold absolute ethanol (<0 °C, 25 mL) and then dried under vacuum for 3 days to yield 0.339 g (0.753 mmol, 75% yield) purple/black solid. The filtrate was concentrated, suspended in cold EtOH, and filtered but yielded no additional product.  $^{51}\text{V}$  NMR in  $\text{CD}_3\text{CN}$ :  $-46$  ppm,  $-10$  ppm (minor isomer).  $^1\text{H}$  NMR (400 MHz,  $\text{CD}_3\text{CN}$ ):  $\delta$  8.71 (s, 1H), 7.69–7.67 (d, 1H), 7.61–7.58 (dd, 1H), 7.56–7.51 (dt, 1H), 6.96–6.92 (dt, 1H), 6.80–6.77 (d, 1H), 6.65 (s, 1H), 6.24 (s, 1H), 5.98–5.95 (s, 1H), 4.49–4.44 (m, 1H), 4.23–4.17 (dd, 1H), 4.10–4.02 (dt, 1H), 3.82–3.74 (m, 1H), 3.70–3.63 (m, 1H), 3.60–3.48 (m, 2H), 3.39–3.31 (m, 1H), 3.04–2.91 (m, 1H), 2.81–2.78 (t, 1H). IR (ATR,  $\text{cm}^{-1}$ ): 1719 (C=O), 1636 (Aromatic), 1289, 1151 (C-O), 955 (V=O). Calc for  $\text{C}_{20}\text{H}_{19}\text{N}_2\text{O}_7\text{V}$ : C, 53.19; H, 4.07; N, 6.06. Found: C, 53.34; H, 4.25; N, 6.22. UV-Vis peaks (in DMSO): 280, 360, and 520 nm.

#### 4.3.5. Preparation of Stock Solution for NMR Spectroscopic Studies

A 20.0 mM stock solution of the respective V-complex was prepared in DMSO by dissolving 0.0580 g, 0.0764 g, 0.0989 g, and 0.0825 g of  $[\text{V}(\text{O})_2(\text{Hshed})]$ ,  $[\text{VO}(\text{Hshed})(\text{cat})]$ ,  $[\text{VO}(\text{Hshed})(\text{dtb})]$ , or  $[\text{VO}(\text{Hshed})(3\text{OMet})]$ , respectively, in 10 mL DMSO. The solution of each V-complex was diluted to form a solution with highest final concentration of 10.0 mM in 50:50 DMSO:H<sub>2</sub>O or 50:50 DMSO:7H9 media.

#### 4.3.6. Preparation of Stock Solutions for Cell Culture Experiments

A 20 mM stock solution of each respective V-complex and its free ligands was prepared in DMSO and diluted with 7H9 media to a concentration of 2.0 mM for biological studies.

#### 4.4. UV-Visible Spectra

Absorbance spectra of V-complexes were measured at 0, 1, 5, and 24 h using a UV-Visible spectrophotometer (BioTek Synergy<sup>TM</sup> HTX Multi-Mode Microplate Reader: Winooski, VT, USA) in the 200 to 800 nm wavelength range. Samples were prepared in solutions of H<sub>2</sub>O:DMSO, 7H9 growth medium:DMSO, or the supernatant fraction obtained from *M. smeg* cell culture.

#### 4.5. Nuclear Magnetic Resonance (NMR) Measurements

$^{51}\text{V}$  NMR using a Bruker 400 MHz spectrometer was used to observe species present at different time points in DMSO:H<sub>2</sub>O samples and DMSO:7H9 medium. Studies of the bacterial supernatant from *M. smeg* culture were attempted as well. Speciation of V-complexes were measured through the integration of the vanadium peaks in the NMR spectra. The stability of the V-complexes and precursor complex  $[\text{V}(\text{O})_2(\text{Hshed})]$  was also checked using  $^{51}\text{V}$  NMR spectroscopy.

#### 4.6. Analysis of Species in Stock Solutions and Media as a Function of Time

The species present were analyzed based on spectroscopic data in aqueous-DMSO solutions and in growth media solutions before and after *M. smeg* growth as described above. The 20.0 mM stock solutions of V-complexes were prepared in DMSO and diluted to the final concentration of 10.0 mM in DI H<sub>2</sub>O (50:50, DMSO:H<sub>2</sub>O) or to the final concentration of 10.0 mM in 7H9 medium (50:50, DMSO:7H9). Samples were incubated at 37 °C during the stability studies. The V-complexes in double-distilled H<sub>2</sub>O and in 7H9 medium (pH 6.65 prior to adding the DMSO solution) were measured at different time points (0, 1, 5, and 24 h) using UV-Vis spectroscopy and  $^{51}\text{V}$  NMR spectroscopy. The UV-Vis spectra were recorded using DMSO:H<sub>2</sub>O (50:50) as a reference and for fresh media and for supernatant previously obtained from *M. smeg* culture. For studies using cell culture supernatant, at each time point (0, 1, 5, and 24 h), a 1 mL aliquot of supernatant was collected from the 5 mL sample for  $^{51}\text{V}$  NMR analysis. The 7H9 media samples measured as a function of time are shown in Figure 4 and others are shown in the Supplementary Materials. The NMR spectra were analyzed by integrating the  $^{51}\text{V}$  NMR spectra and assuming that all



the V-compounds were present as V(V) species. The species present in the spectra were calculated based on the mole fraction of the observed signals and the known concentration of V-complexes added to the solutions.

## 5. Conclusions

The growth effects of an anticancerous non-toxic Schiff base oxido vanadium(V) complex coordinated to 3,5-di-tert-butylcatechol were assessed for comparison to the growth effects a series of subtly different non-toxic compounds using *Mycobacterium smegmatis* (*M. smeg*). We specifically chose to examine (1) the growth effects of Schiff base oxido vanadium complexes coordinated to a catechol and (2) the growth effects of the complexes' respective free catecholates for comparison and to determine (3) when the metal coordination complex is more potent than ligand alone. Schiff base oxido vanadium catecholate compounds are coordination complexes and many of these compounds undergo hydrolysis. To obtain more information on the effects of intact complexes versus ligands, we selected a class of complexes with varying stability that contained a ligand with the potential to inhibit growth of *M. smeg*. We then investigated both the species present under biological conditions and the effects of the intact complex and the hydrolyzed complex as well as the free ligand. The order of growth effects of ligands differed from that of the complexes and complex stability. This did not appear to be critical for growth inhibition because the most inhibitory catechol ligands were not found to form comparably inhibitory complexes. Considering speciation of the V-complex in cell growth medium, we concluded that both hydrophobicity and steric hindrance were important factors for the observed growth inhibition of *M. smeg* as well as the anticancer properties of the various V-complexes.

**Supplementary Materials:** The following supporting information can be downloaded at: <https://www.mdpi.com/article/10.3390/inorganics10040050/s1>, Figure S1: The histograms of the IC<sub>50</sub> values for the effects of the V-complexes; Figure S2: The growth inhibition curves and IC<sub>50</sub> values for the effects of the V-complexes; Figure S3: The growth of *M. smegmatis* in the presence of DMSO; Figure S4: The <sup>51</sup>V NMR spectrum of [VO(Hshed)(4NO<sub>2</sub>)]; Figure S5: The <sup>51</sup>V NMR spectrum of [VO(Hshed)(CN)]; Figure S6: The <sup>51</sup>V NMR spectrum of [VO(Hshed)(3OMet)]; Figure S7: The <sup>51</sup>V NMR spectrum of [VO(Hshed)(Coum)]; Figure S8: The <sup>1</sup>H NMR spectrum of [VO(Hshed)(4NO<sub>2</sub>)]; Figure S9: The <sup>1</sup>H NMR spectrum of [VO(Hshed)(CN)]; Figure S10: The <sup>1</sup>H NMR spectrum of [VO(Hshed)(3OMet)]; Figure S11: The <sup>1</sup>H NMR spectrum of [VO(Hshed)(Coum)]; Figure S12: The IR spectrum of [VO(Hshed)(4NO<sub>2</sub>)]; Figure S13: The IR spectrum of [VO(Hshed)(CN)]; Figure S14: The IR spectrum of [VO(Hshed)(3OMet)]; Figure S15: The IR spectrum of [VO(Hshed)(Coum)]; Figure S16: The UV-vis spectrum of [VO(Hshed)(4NO<sub>2</sub>)]; Figure S17: The UV-vis spectrum of [VO(Hshed)(CN)]; Figure S18: The UV-vis spectrum of [VO(Hshed)(3OMet)]; Figure S19: The UV-vis spectrum of [VO(Hshed)(Coum)]; Figure S20: The UV-vis spectra are recorded of all the complexes at 0.250 mM in ddH<sub>2</sub>O as a function of time (0, 1, 5, 24 h); Figure S21: The UV-vis spectra are recorded of all the complexes at 0.250 mM in supernatant fraction as a function of time (0, 1, 5, 24 h); Figure S22: The UV-vis spectra are recorded of all the free ligands at 0.250 mM in ddH<sub>2</sub>O and 7H9 medium at time zero (0 h); Figure S23: The <sup>51</sup>V NMR spectra of 10 mM [VO(Hshed)(3OMet)] at 0, 1, 5, and 24 h time points in a) 50:50 H<sub>2</sub>O:DMSO and in b) 50:50 7H9 growth medium: DMSO; Figure S24: The <sup>51</sup>V NMR spectra of 10 mM [VO(Hshed)(tbc)] at 0, 1, 5, and 24 h time points in a) 50:50 H<sub>2</sub>O:DMSO and in b) 50:50 7H9 growth medium: DMSO; Figure S25: The <sup>51</sup>V NMR spectra of 10 mM [VO(Hshed)(4NO<sub>2</sub>)] at 0, 1, 5, and 24 h time points in a) 50:50 H<sub>2</sub>O:DMSO and in b) 50:50 7H9 growth medium: DMSO; Figure S26: The <sup>51</sup>V NMR spectra of 10 mM [VO(Hshed)(CN)] at 0, 1, 5, and 24 h time points in a) 50:50 H<sub>2</sub>O:DMSO and in b) 50:50 7H9 growth medium: DMSO; Figure S27: The <sup>51</sup>V NMR spectra of 10 mM [VO(Hshed)(Coum)] at 0, 1, 5, and 24 h time points in a) 50:50 H<sub>2</sub>O:DMSO and in b) 50:50 7H9 growth medium: DMSO; Figure S28: The <sup>51</sup>V NMR spectra of 10 mM [VO(Hshed)(dtb)] at 0, 1, 5, and 24 h time points in supernatant fraction; Figure S29: The <sup>51</sup>V NMR spectra of 10 mM [VO(Hshed)(cat)] at 0, 1, 5, and 24 h time points in supernatant fraction; Figure S30: The <sup>51</sup>V NMR spectra of 10 mM [V(O)<sub>2</sub>(Hshed)] at 0, 1, 5, and 24 h time points in supernatant fraction; Figure S31: The <sup>51</sup>V NMR spectra of 10 mM [VO(Hshed)(3OMet)] at 0, 1, 5, and 24 h time points in supernatant fraction.



**Author Contributions:** Conceptualization, D.C.C. (Debbie C. Crans) and Z.A.; data curation, Z.A. and D.C.C. (Debbie C. Crans); formal analysis, Z.A., J.T.K., X.L., H.A.M., D.C.C. (Dean C. Crick), and D.C.C. (Debbie C. Crans); funding acquisition, D.C.C. (Debbie C. Crans); investigation, Z.A., J.T.K., X.L. and H.A.M.; methodology, Z.A., J.T.K., D.C.C. (Dean C. Crick) and D.C.C. (Debbie C. Crans); project administration, D.C.C. (Debbie C. Crans); supervision, D.C.C. (Debbie C. Crans); validation, Z.A., J.T.K., D.C.C. (Dean C. Crick) and D.C.C. (Debbie C. Crans); writing—original draft, Z.A., D.A.R., and D.C.C. (Debbie C. Crans); writing—review and editing, Z.A., D.A.R. and D.C.C. (Debbie C. Crans). All authors have read and agreed to the published version of the manuscript.

**Funding:** D.C. Crans thanks the Arthur Cope Foundation administered by the American Chemical Society and Colorado State University for support.

**Institutional Review Board Statement:** Not applicable.

**Informed Consent Statement:** Not applicable.

**Data Availability Statement:** See Supplementary Materials where additional data pertinent to this study is collected.

**Acknowledgments:** The authors thank Christopher D. Rithner from the Central Instrumentation Facility (the CIF) and the renamed facility now named the ARC for assistance with the NMR studies.

**Conflicts of Interest:** The authors declare no conflict of interest. The funders were not involved in the design, the collection, the analyses, or the interpretation of data. The funders were also not involved in the writing of the manuscript, or in the decision to publish the results.

## Abbreviations

cat:	Catechol
Coum	6,7-Dihydroxycoumarin
DMSO	Dimethylsulfoxide
dtb	3,4-Ditertbutyl catechol
IC <sub>50</sub>	Concentration at 50% growth inhibition
<i>M. smeg</i>	<i>Mycobacterium smegmatis</i>
NMR	Nuclear Magnetic Resonance
OD	Optical density
CN	3,4-Dihydroxybenzonitrile
tbc	Tetrabromocatechol
UV-Vis	Ultraviolet-visible spectroscopy
V	Vanadium
V <sub>1</sub>	Vanadate monomer
V <sub>4</sub>	Vanadate tetramer
V-complexes,	Vanadium complexes
[VO(Hshed)(3OMet)]	see Figure 2
[VO(Hshed)(4NO <sub>2</sub> )]	see Figure 2
[VO(Hshed)(cat)]	see Figure 2
[VO(Hshed)(CN)]	see Figure 2
[VO(Hshed)(Coum)]	see Figure 2
[VO(Hshed)(dtb)]	see Figure 2
[VO(Hshed)(tbc)]	see Figure 2
3OMet	3-methoxycatechol
4NO <sub>2</sub>	4-nitrocatechol

## References

1. Cirri, D.; Bartoli, F.; Pratesi, A.; Baglini, E.; Barresi, E.; Marzo, T. Strategies for the Improvement of Metal-Based Chemotherapeutic Treatments. *Biomedicines*. **2021**, *9*, 504. [[CrossRef](#)] [[PubMed](#)]
2. Dasari, S.; Tchounwou, P.B. Cisplatin in cancer therapy: Molecular mechanisms of action. *Eur. J. Pharmacol.* **2014**, *740*, 364–378. [[CrossRef](#)] [[PubMed](#)]
3. Dilruba, S.; Kalayda, G.V. Platinum-based drugs: Past, present and future. *Cancer Chemother. Pharmacol.* **2016**, *77*, 1103–1124. [[CrossRef](#)] [[PubMed](#)]

4. Graf, N.; Lippard, S.J. Redox activation of metal-based prodrugs as a strategy for drug delivery. *Adv. Drug Deliv. Rev.* **2012**, *64*, 993–1004. [[CrossRef](#)]
5. Jin, S.; Guo, Y.; Guo, Z.; Wang, X. Monofunctional Platinum(II) Anticancer Agents. *Pharmaceuticals* **2021**, *14*, 133. [[CrossRef](#)]
6. Johnstone, T.C.; Wilson, J.J.; Lippard, S.J. Monofunctional and higher-valent platinum anticancer agents. *Inorg. Chem.* **2013**, *52*, 12234–12249. [[CrossRef](#)]
7. Xu, Z.F.; Wang, Z.G.; Deng, Z.Q.; Zhu, G.Y. Recent advances in the synthesis, stability, and activation of platinum (IV) anticancer prodrugs. *Coord. Chem. Rev.* **2021**, *442*, 213991. [[CrossRef](#)]
8. Rottenberg, S.; Disler, C.; Perego, P. The rediscovery of platinum-based cancer therapy. *Nat. Rev. Cancer* **2021**, *21*, 37–50. [[CrossRef](#)]
9. Zhou, J.B.; Kang, Y.; Chen, L.; Wang, H.; Liu, J.Q.; Zeng, S.; Yu, L.S. The Drug-Resistance Mechanisms of Five Platinum-Based Antitumor Agents. *Front. Pharmacol.* **2020**, *11*, 343. [[CrossRef](#)]
10. Thota, S.; Rodrigues, D.A.; Crans, D.C.; Barreiro, E.J. Ru(II) Compounds: Next-Generation Anticancer Metallotherapeutics? *J. Med. Chem.* **2018**, *61*, 5805–5821. [[CrossRef](#)]
11. Manov, H.; Staneva, D.; Vasileva-Tonkova, E.; Alexandrova, R.; Stoyanova, R.; Kukeva, R.; Stoyanov, S.; Grabchev, I. A New Cu(II) Complex of PAMAM Dendrimer Modified with 1,8-Naphthalimide: Antibacterial and Anticancer Activity. *Biointerface Res. Appl. Chem.* **2022**, *12*, 5534–5547. [[CrossRef](#)]
12. Crans, D.C.; Yang, L.N.; Haase, A.; Yang, X.G. Health Benefits of Vanadium and Its Potential as an Anticancer Agent. *Metal Ions Life Sci.* **2018**, *18*, 251–280. [[CrossRef](#)]
13. Selman, M.; Rouso, C.; Bergeron, A.; Son, H.H.; Krishnan, R.; El-Sayes, N.A.; Varette, O.; Chen, A.; Le Boeuf, F.; Tzelepis, F.; et al. Multi-modal Potentiation of Oncolytic Virotherapy by Vanadium Compounds. *Mol. Ther.* **2018**, *26*, 56–69. [[CrossRef](#)] [[PubMed](#)]
14. Crans, D.C.; Kostenkova, K. Open questions on the biological roles of first-row transition metals. *Commun. Chem.* **2020**, *3*, 104. [[CrossRef](#)]
15. Shahbazi, M.A.; Faghfour, L.; Ferreira, M.P.A.; Figueiredo, P.; Maleki, H.; Sefat, F.; Hirvonen, J.; Santos, H.A. The versatile biomedical applications of bismuth-based nanoparticles and composites: Therapeutic, diagnostic, biosensing, and regenerative properties. *Chem. Soc. Rev.* **2020**, *49*, 1253–1321. [[CrossRef](#)]
16. Fernandes, N.; Rodrigues, C.F.; Moreira, A.F.; Correia, I.J. Overview of the application of inorganic nanomaterials in cancer photothermal therapy. *Biomater. Sci.* **2020**, *8*, 2990–3020. [[CrossRef](#)]
17. Bauer, E.B.; Haase, A.A.; Reich, R.M.; Crans, D.C.; Kuhn, F.E. Organometallic and coordination rhenium compounds and their potential in cancer therapy. *Coord. Chem. Rev.* **2019**, *393*, 79–117. [[CrossRef](#)]
18. Needham, R.J.; Prokes, I.; Habtemariam, A.; Romero-Canelon, I.; Clarkson, G.J.; Sadler, P.J. NMR studies of group 8 metallodrugs: Os-187-enriched organo-osmium half-sandwich anticancer complex. *Dalton Trans.* **2021**, *50*, 12970–12981. [[CrossRef](#)]
19. Frei, A.; Zuegg, J.; Elliott, A.G.; Baker, M.; Braese, S.; Brown, C.; Chen, F.; Dowson, C.G.; Dujardin, G.; Jung, N.; et al. Metal complexes as a promising source for new antibiotics. *Chem. Sci.* **2020**, *11*, 2627–2639. [[CrossRef](#)]
20. Imberti, C.; Sadler, P.J. 150 years of the periodic table: New medicines and diagnostic agents. *Adv. Inorg. Chem.* **2020**, *75*, 3–56. [[CrossRef](#)]
21. Eyvazi, S.; Vostakolaei, M.A.; Dilmaghani, A.; Borumandi, O.; Hejazi, M.S.; Kahroba, H.; Tarhriz, V. The oncogenic roles of bacterial infections in development of cancer. *Microb. Pathog.* **2020**, *141*, 104019. [[CrossRef](#)] [[PubMed](#)]
22. Pulcini, C.D.; Lentz, S.; Saladino, R.A.; Bounds, R.; Herrington, R.; Michaels, M.G.; Maurer, S.H. Emergency management of fever and neutropenia in children with cancer: A review. *Am. J. Emerg. Med.* **2021**, *50*, 693–698. [[CrossRef](#)] [[PubMed](#)]
23. Ross, J.A.; Komoda, K.; Pal, S.; Dickter, J.; Salgia, R.; Dadwal, S. Infectious complications of immune checkpoint inhibitors in solid organ malignancies. *Cancer Med.* **2022**, *11*, 21–27. [[CrossRef](#)]
24. Rossi, J.F.; Lu, Z.Y.; Massart, C.; Levon, K. Dynamic Immune/Inflammation Precision Medicine: The Good and the Bad Inflammation in Infection and Cancer. *Front. Immunol.* **2021**, *12*, 97. [[CrossRef](#)] [[PubMed](#)]
25. Doucette, K.A.; Hassell, K.N.; Crans, D.C. Selective speciation improves efficacy and lowers toxicity of platinum anticancer and vanadium antidiabetic drugs. *J. Inorg. Biochem.* **2016**, *165*, 56–70. [[CrossRef](#)] [[PubMed](#)]
26. Esteban-Fernandez, D.; Moreno-Gordaliza, E.; Canas, B.; Palacios, M.A.; Gomez-Gomez, M.M. Analytical methodologies for metallomics studies of antitumor Pt-containing drugs. *Metallomics* **2010**, *2*, 19–38. [[CrossRef](#)]
27. Levina, A.; Crans, D.C.; Lay, P.A. Speciation of metal drugs, supplements and toxins in media and bodily fluids controls in vitro activities. *Coord. Chem. Rev.* **2017**, *352*, 473–498. [[CrossRef](#)]
28. Nunes, P.; Correia, I.; Cavaco, I.; Marques, F.; Pinheiro, T.; Avecilla, F.; Pessoa, J.C. Therapeutic potential of vanadium complexes with 1,10-phenanthroline ligands, quo vadis? Fate of complexes in cell media and cancer cells. *J. Inorg. Biochem.* **2021**, *217*, 111350. [[CrossRef](#)] [[PubMed](#)]
29. Wexselblatt, E.; Yavin, E.; Gibson, D. Platinum(IV) prodrugs with haloacetato ligands in the axial positions can undergo hydrolysis under biologically relevant conditions. *Angew. Chem. Int. Ed. Engl.* **2013**, *52*, 6059–6062. [[CrossRef](#)]
30. Loizou, M.; Hadjiadamou, I.; Drouza, C.; Keramidas, A.D.; Simos, Y.V.; Peschos, D. Vanadium(V) Complexes with Siderophore Vitamin E-Hydroxylamino-Triazine Ligands. *Inorganics* **2021**, *9*, 73. [[CrossRef](#)]
31. Creaven, B.S.; Duff, B.; Egan, D.A.; Kavanagh, K.; Rosair, G.; Thangella, V.R.; Walsh, M. Anticancer and antifungal activity of copper(II) complexes of quinolin-2(1H)-one-derived Schiff bases. *Inorg. Chim. Acta* **2010**, *363*, 4048–4058. [[CrossRef](#)]

32. Correia, I.; Adao, P.; Roy, S.; Wahba, M.; Matos, C.; Maurya, M.R.; Marques, F.; Pavan, F.R.; Leite, C.Q.F.; Avecilla, F.; et al. Hydroxyquinoline derived vanadium(IV and V) and copper(II) complexes as potential anti-tuberculosis and anti-tumor agents. *J. Inorg. Biochem.* **2014**, *141*, 83–93. [\[CrossRef\]](#)
33. Crans, D.C.; Koehn, J.T.; Petry, S.M.; Glover, C.M.; Wijetunga, A.; Kaur, R.; Levina, A.; Lay, P.A. Hydrophobicity may enhance membrane affinity and anti-cancer effects of Schiff base vanadium(v) catecholates complexes. *Dalton Trans.* **2019**, *48*, 6383–6395. [\[CrossRef\]](#) [\[PubMed\]](#)
34. Levina, A.; Pires Vieira, A.; Wijetunga, A.; Kaur, R.; Koehn, J.T.; Crans, D.C.; Lay, P.A. A Short-Lived but Highly Cytotoxic Vanadium(V) Complex as a Potential Drug Lead for Brain Cancer Treatment by Intratumoral Injections. *Angew. Chem. Int. Ed. Engl.* **2020**, *59*, 15834–15838. [\[CrossRef\]](#) [\[PubMed\]](#)
35. Maurya, M.R.; Khan, A.A.; Azam, A.; Ranjan, S.; Mondal, N.; Kumar, A.; Avecilla, F.; Pessoa, J.C. Vanadium complexes having [(VO)-O-IV]<sup>2+</sup> and [(VO2)-O-V]<sup>+</sup> cores with binucleating dibasic tetradentate ligands: Synthesis, characterization, catalytic and antiamoebic activities. *Dalton Trans.* **2010**, *39*, 1345–1360. [\[CrossRef\]](#)
36. Rosu, T.; Pahontu, E.; Ilies, D.C.; Georgescu, R.; Mocanu, M.; Leabu, M.; Shova, S.; Gulea, A. Synthesis and characterization of some new complexes of Cu(II), Ni(II) and V(IV) with Schiff base derived from indole-3-carboxaldehyde. Biological activity on prokaryotes and eukaryotes. *Eur. J. Med. Chem.* **2012**, *53*, 380–389. [\[CrossRef\]](#) [\[PubMed\]](#)
37. Machado Pde, A.; Mota, V.Z.; Cavalli, A.C.; de Carvalho, G.S.; Da Silva, A.D.; Gameiro, J.; Cuin, A.; Coimbra, E.S. High selective antileishmanial activity of vanadium complex with stilbene derivative. *Acta Trop.* **2015**, *148*, 120–127. [\[CrossRef\]](#) [\[PubMed\]](#)
38. He, L.Y.; Qiu, X.Y.; Cheng, J.Y.; Liu, S.J.; Wu, S.M. Synthesis, characterization and crystal structures of vanadium(V) complexes derived from halido-substituted tridentate hydrazone compounds with antimicrobial activity. *Polyhedron* **2018**, *156*, 105–110. [\[CrossRef\]](#)
39. Missina, J.M.; Gavinho, B.; Postal, K.; Santana, F.S.; Valdameri, G.; de Souza, E.M.; Hughes, D.L.; Ramirez, M.I.; Soares, J.F.; Nunes, G.G. Effects of Decavanadate Salts with Organic and Inorganic Cations on *Escherichia coli*, *Giardia intestinalis*, and Vero Cells. *Inorg. Chem.* **2018**, *57*, 11930–11941. [\[CrossRef\]](#) [\[PubMed\]](#)
40. Costello, R.L.; Hedgecock, L.W. Effect of metavanadate ion on the growth in vitro of *Mycobacterium tuberculosis*. *J. Bacteriol.* **1959**, *77*, 794–799. [\[CrossRef\]](#)
41. Samart, N.; Arhouma, Z.; Kumar, S.; Murakami, H.A.; Crick, D.C.; Crans, D.C. Decavanadate Inhibits *Mycobacterial* Growth More Potently Than Other Oxovanadates. *Front. Chem.* **2018**, *6*, 519. [\[CrossRef\]](#) [\[PubMed\]](#)
42. Kostenkova, K.; Arhouma, Z.; Postal, K.; Rajan, A.; Kortz, U.; Nunes, G.G.; Crick, D.C.; Crans, D.C. Pt(IV)- or Mo(VI)-substituted decavanadates inhibit the growth of *Mycobacterium smegmatis*. *J. Inorg. Biochem.* **2021**, *217*, 111356. [\[CrossRef\]](#)
43. Mosquillo, M.F.; Smircich, P.; Lima, A.; Gehrke, S.A.; Scalese, G.; Machado, I.; Gambino, D.; Garat, B.; Perez-Diaz, L. High Throughput Approaches to Unravel the Mechanism of Action of a New Vanadium-Based Compound against *Trypanosoma cruzi*. *Bioinorg. Chem. Appl.* **2020**, *2020*, 1634270. [\[CrossRef\]](#) [\[PubMed\]](#)
44. Griffin, E.; Levina, A.; Lay, P.A. Vanadium(V) tris-3,5-di-tert-butylcatecholato complex: Links between speciation and anti-proliferative activity in human pancreatic cancer cells. *J. Inorg. Biochem.* **2019**, *201*, 110815. [\[CrossRef\]](#)
45. Lima, L.M.A.; Murakami, H.; Gaebler, D.J.; Silva, W.E.; Belian, M.F.; Lira, E.C.; Crans, D.C. Acute Toxicity Evaluation of Non-Innocent Oxidovanadium(V) Schiff Base Complex. *Inorganics* **2021**, *9*, 42. [\[CrossRef\]](#)
46. Chen, X.; Hu, X.; Lu, Q.; Yang, Y.; Linghu, S.; Zhang, X. Study on the differences in sludge toxicity and microbial community structure caused by catechol, resorcinol and hydroquinone with metagenomic analysis. *J. Environ. Manag.* **2022**, *302*, 114027. [\[CrossRef\]](#) [\[PubMed\]](#)
47. Lambert de Malezieu, M.; Courtel, P.; Sleno, L.; Abasq, M.L.; Ramassamy, C. Synergistic properties of bioavailable phenolic compounds from olive oil: Electron transfer and neuroprotective properties. *Nutr. Neurosci.* **2021**, *24*, 660–673. [\[CrossRef\]](#)
48. Schweigert, N.; Zehnder, A.J.B.; Eggen, R.I.L. Chemical properties of catechols and their molecular modes of toxic action in cells, from microorganisms to mammals. *Environ. Microbiol.* **2001**, *3*, 81–91. [\[CrossRef\]](#) [\[PubMed\]](#)
49. Chaturvedi, S.K.; Ahmad, E.; Khan, J.M.; Alam, P.; Ishtikhar, M.; Khan, R.H. Elucidating the interaction of limonene with bovine serum albumin: A multi-technique approach. *Mol. Biosyst.* **2015**, *11*, 307–316. [\[CrossRef\]](#)
50. Ribeiro, N.; Bulut, I.; Cevatemre, B.; Teixeira, C.; Yildizhan, Y.; Andre, V.; Adao, P.; Pessoa, J.C.; Acilan, C.; Correia, I. Cu(II) and V(IV)O complexes with tri- or tetradentate ligands based on (2-hydroxybenzyl)-L-alanines reveal promising anticancer therapeutic potential. *Dalton Trans.* **2021**, *50*, 157–169. [\[CrossRef\]](#)
51. Le, M.; Rathje, O.; Levina, A.; Lay, P.A. High cytotoxicity of vanadium(IV) complexes with 1,10-phenanthroline and related ligands is due to decomposition in cell culture medium. *J. Biol. Inorg. Chem.* **2017**, *22*, 663–672. [\[CrossRef\]](#) [\[PubMed\]](#)
52. Pessoa, J.C.; Santos, M.F.A.; Correia, I.; Sanna, D.; Sciortino, G.; Garribba, E. Binding of vanadium ions and complexes to proteins and enzymes in aqueous solution. *Coord. Chem. Rev.* **2021**, *449*, 214192. [\[CrossRef\]](#)
53. Aureliano, M.; Gumerova, N.I.; Sciortino, G.; Garribba, E.; McLauchlan, C.C.; Rempel, A.; Crans, D.C. Polyoxidovanadates' interactions with proteins: An overview. *Coord. Chem. Rev.* **2022**, *454*, 214344. [\[CrossRef\]](#)
54. Haase, A.A.; Murakami, H.A.; Koehn, J.T.; Hagan, J.; Beuning, C.N.; Levina, A.; Lay, P.A.; Crans, D.C. Exploring Electronic Properties of New Non-Innocent Vanadium(V) Compounds. 2022; under preparation.
55. Kumar, S.; Koehn, J.T.; Gonzalez-Juarrero, M.; Crans, D.C.; Crick, D.C. *Mycobacterium tuberculosis* Survival in J774A.1 Cells Is Dependent on MenJ Moonlighting Activity, not Its Enzymatic Activity. *Acs Infect. Dis.* **2020**, *6*, 2661–2671. [\[CrossRef\]](#) [\[PubMed\]](#)

- 
56. Cornman, C.R.; Colpas, G.J.; Hoeschele, J.D.; Kampf, J.; Pecoraro, V.L. Implications for the Spectroscopic Assignment of Vanadium Biomolecules—Structural and Spectroscopic Characterization of Monooxovanadium(V) Complexes Containing Catecholate and Hydroximate Based Noninnocent Ligands. *J. Am. Chem. Soc.* **1992**, *114*, 9925–9933. [[CrossRef](#)]
  57. Chatterjee, P.B.; Goncharov-Zapata, O.; Quinn, L.L.; Hou, G.; Hamaed, H.; Schurko, R.W.; Polenova, T.; Crans, D.C. Characterization of noninnocent metal complexes using solid-state NMR spectroscopy: O-dioxolene vanadium complexes. *Inorg. Chem.* **2011**, *50*, 9794–9803. [[CrossRef](#)] [[PubMed](#)]
  58. Goncharova-Zapata, O.; Chatterjee, P.B.; Hou, G.; Quinn, L.L.; Li, M.; Yehl, J.; Crans, D.C.; Polenova, T. Effect of Ancillary Ligand on Electronic Structure as Probed by (51)V Solid-State NMR Spectroscopy for Vanadium-o-Dioxolene Complexes. *CrystEngComm* **2013**, *15*, 8776–8783. [[CrossRef](#)] [[PubMed](#)]